



NTNU – Trondheim
Norwegian University of
Science and Technology

Thermal flow in fractured porous media and operator splitting

Joachim Dyrdaahl

Master of Science in Mathematics

Submission date: June 2014

Supervisor: Helge Holden, MATH

Co-supervisor: Atgeirr Rasmussen, SINTEF

Norwegian University of Science and Technology
Department of Mathematical Sciences

Abstract

Thermal flow in fractured porous medium is an area of interest for both the oil and the geothermal energy industry. The mathematical model consists of multiple equations, often various conservation laws and constitutive relations. Solving these equations simultaneously is called the fully implicit approach, an alternative is sequential splitting. We investigate and compare these approaches, applied on incompressible and compressible cases of single-phase and two-phase fluid flow. The experiments show that the difference of the solutions between our approaches is small, and that the results from the sequentially split solver are obtained significantly faster than the fully implicit solver scheme.

Contents

1	Introduction	6
2	Geothermal Energy	8
3	Flow in Porous Media	9
3.1	General properties	9
3.1.1	Porosity	9
3.1.2	Permeability	10
3.1.3	Density	11
3.1.4	Compressibility	11
3.1.5	Thermal Expansion Coefficient	11
3.1.6	Incompressible Flow	11
3.1.7	Viscosity	11
3.2	Multiphase Flow Variables	12
3.2.1	Fluid Phases	12
3.2.2	Saturation	12
3.2.3	Capillary Pressure	13
3.2.4	Relative Permeability	13
3.2.5	Mobility	13
4	Continuum Mechanics	13
4.1	Conservation of Mass	14
4.2	Darcy's Law	15
4.3	Two-Phase Flow	17
5	Thermal Flow	19
5.1	Energy, Heat and Work	19
5.2	Heat Transfer	20
5.2.1	Conduction	20
5.2.2	Convection	21
5.3	Specific Heat Capacity	22
5.4	Entropy	22
5.5	Internal Energy	23
5.6	Enthalpy	23
5.7	Energy Equation	24
5.8	Final Set of Equations	27
6	Fractures	28
6.1	Fracture Models	28
6.2	Flow in Fractures	30

7	Numerics	33
7.1	Spatial Discretisation	34
7.1.1	Finite Volume Methods	34
7.1.2	Upstream Method	37
7.2	Temporal Discretisation	38
7.2.1	Finite Difference Methods	38
7.3	Numerical Solvers	39
7.3.1	Linear Solver	40
7.3.2	Non-Linear Solver	41
7.4	Automatic Differentiation	42
7.5	Discretising Equations	42
7.5.1	Source Term	46
7.6	Energy equations	47
7.6.1	Spatial Term	48
7.6.2	Source Term	49
7.6.3	Temporal Term	49
8	Operator splitting	50
8.1	Background/Motivation	50
8.2	Application	51
9	Experiments	52
9.1	Environment Specifications	52
9.2	MRST	52
9.3	Add-On Modules	52
9.4	Model Description	53
9.4.1	Grid	53
9.4.2	Wells	56
9.4.3	Aperture function	56
9.4.4	Viscosity	56
9.4.5	Temperature settings	58
9.4.6	Rock properties	58
9.4.7	Time keeping routines	58
9.4.8	Evaluation of temperature solutions	59
9.4.9	Additional Assumptions	59
9.5	Single-Phase Incompressible Flow	59
9.6	Single-Phase Compressible flow	60
9.7	Two-Phase Incompressible Flow	60
9.8	Two-Phase Compressible Flow	72
10	Conclusion	75

References	77
Appendices	79

Preface

Developing reliable and renewable sources of energy is the key to a sustainable future. Geothermal energy is a reliable, renewable and *local* source of energy. To have any contribution to this field has been the motivation for this thesis.

I would very much like to thank my supervisors Atgeirr Rasmussen (SINTEF) and Helge Holden (NTNU) for counselling and guidance. A huge thanks goes to all at SINTEF Applied Mathematics, especially Knut-Andreas Lie for giving me this opportunity and Halvor Møll Nilsen for sharing his code and his understanding of physical phenomena.

In addition, a special thanks goes to Sindre Hilden for sharing his office and his knowledge during this period.

1 Introduction

In the last decades, extensive research has been done in the field of porous media flow. First and foremost for the oil and gas industry, but also for the modelling of groundwater basins and geothermal energy resources. At the same time, having access to increasingly powerful computers has made us able to solve increasingly complex mathematical models. This has in turn led to a need for more efficient solver routines. Operator splitting techniques come as a response to this need, rigorous work has been done in this field, see for example Holden et al [8].

Thermal flow in fractured porous media is an example of such a complex model. The model is relevant for many purposes, but the main focus here is on its geothermal energy applications. In this thesis we will construct the model, solve it using two different approaches and then compare the results.

Outline

We will investigate thermal flow in fractured porous media and apply an operator splitting technique to the fully implicit solver based on Automatic Differentiation (AD). This requires an initial discussion of a number of subjects and the definition of key concepts. Below is an outline of the chapters in this thesis.

Chapter 2 - Geothermal Energy

Contains an introduction to the subject and some production techniques.

Chapter 3 - Flow in Porous Media

In this chapter we define basic and derived properties of rock, fluid and concepts related to flow of one and more phases in porous media.

Chapter 4 - Continuum Mechanics

Starting out from the principle of mass conservation, we derive the continuity equation and the Darcy flow velocity for porous media. We then expand the equations to govern a multiphase flow.

Chapter 5 - Thermal Flow

Basic concepts of thermodynamics are defined. We then apply the conservation principle to energy and derive a multiphase equation for thermal flow.

Chapter 6 - Fractures

Some fracture models are defined, and we make a choice of model to pursue. For our model, we consider mass flow mainly in fractures.

Chapter 7 - Numerics

In order to solve the derived analytic equations, we need a number of numeric methods. These methods are described in this chapter, before applying them to our equations.

Chapter 8 - Operator Splitting

Here we discuss the background and motivation for applying operator splitting techniques, and give a general outline of the method.

Chapter 9 - Experiments

Given all of the above, we are now able to implement and run the experiments in MATLAB. We discuss these as the results are given, the details of these and some thoughts of future work are also included here.

Chapter 10 - Conclusion

Here we give the conclusion of the work and discussion in Chapter 9.

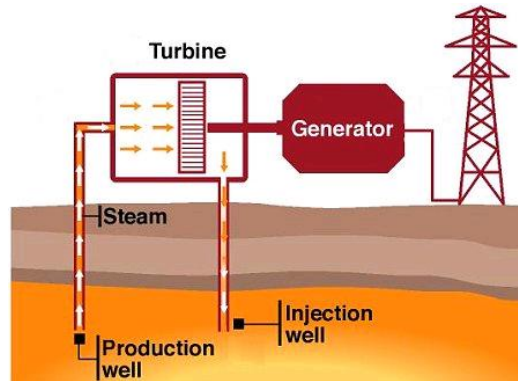


Figure 1: Schematic geothermal powerplant (EDEN project 2012)

2 Geothermal Energy

Geothermal energy is thermal energy generated by radioactive processes in the planet core. There are two main methods of collecting this energy, either through capturing heat at natural hot springs and through extraction of heat from hot dry rock(HDR) formations.

Hot Dry Rock is a collective term for underground rock formations with a temperature around 150-200 degrees Celsius[4]. Conceptually, HDR heat extraction is quite simple. Cold water is pumped down into the crust via an injection well, it becomes superheated as it flows through fractures in the hot rock reservoir, and is returned to the surface through production wells. At the surface the heat is extracted and through conventional power plants turned into electricity, while the cooled water is led back into the ground through the injection well, repeating the procedure.

In areas where the natural fractures and pore connectivity do not allow sufficient flow rates, the permeability can be enhanced by pumping high-pressure cold water down an injection well into the rock. The injection increases the fluid pressure in the naturally fractured rock, stimulating events that enhance the system's permeability, and is substantially the same as hydraulic tensile fracturing used in the oil and gas industry.

There are three basic types of geothermal power plants:

- *Dry Steam plants* use steam piped directly from a geothermal reservoir to turn the generator turbines. The first geothermal power plant was built in 1904 in Tuscany, Italy, where natural steam erupted from the Earth.
- *Flash Steam plants* take high-pressure hot water from deep inside the Earth and convert it to steam to drive the generator turbines. When

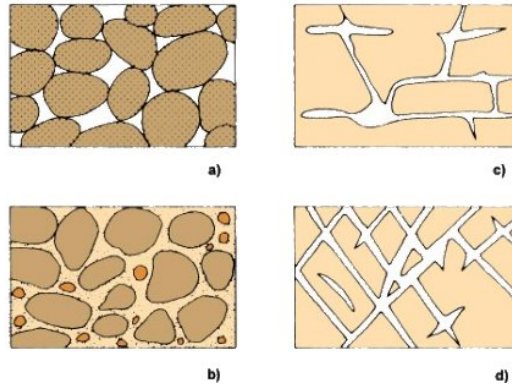


Figure 2: Porosity

the steam cools, it condenses to water and is injected back into the ground to be used over and over again. Most geothermal power plants are flash steam plants.

- *Binary Cycle Power plants* transfer the heat from geothermal hot water to another liquid. The heat causes the second liquid to turn to steam which is used to drive a generator turbine.

3 Flow in Porous Media

Most materials in nature can be considered as porous, meaning they are a composition of voids and solid parts. The non-penetrable part of the material is hereafter called the *matrix*, and the voids are called *pores*, with respective volumes, V_M and, V_P . The total volume, $V_B = V_P + V_M$, of the medium is called the *bulk* volume.

The type of flow that will be discussed hereafter occurs in materials with connected voids of very small diameters, typically $< 0.1\text{mm}$. On this scale, friction between the fluid and solid is a dominating effect, flow velocities are low and is thus governed by its own set of equations. Flow in these types of media will occur in various manners; Figure 2 a) and b) shows the structure of sandstone, here the flow takes place between more or less loosely consolidated grains, whilst Figure 2 c) and d) displays limestone, where the fluid flows within channel-looking structures.

3.1 General properties

3.1.1 Porosity

The ratio of pore and total volume in a material is called the *porosity*, ϕ , of the medium,

$$\phi = \frac{V_P}{V_B},$$

and is used a measure of the medium's ability to *store* a fluid. ϕ is dimensionless, and always a positive number between 0 and 1. As examples, *granite* will have a porosity around 0.01 while a *sponge* is likely have a porosity close to 1.

3.1.2 Permeability

Permeability, \mathbf{K} , describes the medium's ability to *transfer* a fluid at a given state. It is therefore strongly correlated to porosity, but there is no direct relation between the two. If a rock formation has a well connected pore system and transmits fluid well, we say that the rock is *permeable*. The SI unit of \mathbf{K} is m^2 , but it is normally expressed in the unit *Darcy*, D.

The system permeability is a tensor, expressed as a 3x3 matrix. It is common to simplify the model by shifting the basis and disregard permeability variations in all other directions than in the directions given along the axis of the usual three spatial dimensions. Further, we can simplify the system by regarding the medium as isotropic, i.e. we regard \mathbf{K} as a scalar function. In these models the permeability for the horizontal directions is the same as for the vertical.

Pressure and temperature are also important factors for determining permeability, when these change during production, fractures may open or friction between formation and fluid might change. Also, since the definition of permeability involves a fluid, different fluids can experience different permeabilities during flow in the same formation.

3.1.3 Density

For all materials we define the property of density, ρ , as mass per unit volume,

$$\rho = \frac{m}{V}.$$

The corresponding SI unit is kg/m^3 .

3.1.4 Compressibility

The compressibility factor, c is a measure of change in the material volume V per volume unit ;

$$c = -\frac{1}{V} \frac{\partial V}{\partial p} = \frac{1}{\rho} \frac{\partial \rho}{\partial p}. \quad (1)$$

3.1.5 Thermal Expansion Coefficient

The thermal expansion coefficient is defined similarly, and is a measure of how volume changes with temperature;

$$\beta = \frac{1}{V} \frac{\partial V}{\partial T} = -\frac{1}{\rho} \frac{\partial \rho}{\partial T}. \quad (2)$$

3.1.6 Incompressible Flow

We distinguish between incompressible and compressible fluids. A fluid is considered incompressible if its density does not change with pressure. In other words, the density of fluid particles does not change, but different fluid particles may have different density. In mathematical terms,

$$\frac{D\rho}{Dt} \equiv \frac{\partial \rho}{\partial t} + \mathbf{u} \cdot \nabla \rho = 0, \quad (3)$$

hence, the flow is said to be incompressible if $\frac{D\rho}{Dt} = 0$, and *steady* if ρ and \mathbf{u} are independent of t . Density is often a function of pressure and temperature, but for fluid flow in porous media with water phase only, it is common to neglect these effects.

3.1.7 Viscosity

Flow can be interpreted as a continuous *deformation* of fluid due to stress. The viscosity, μ , of a fluid, is the measure of how much a fluid will resist this deformation. To clarify, a highly viscous fluid will move slower than a less viscous fluid. Viscosity of a fluid depends on both temperature and pressure, hence $\mu = \mu(p, T)$. A more detailed description is included in chapter 9.

3.2 Multiphase Flow Variables

3.2.1 Fluid Phases

In reservoir simulation, it is common to categorize fluids into one of three different *phases*, α : aqueous(w), oleic(o) and gaseous(g) phase. Each phase

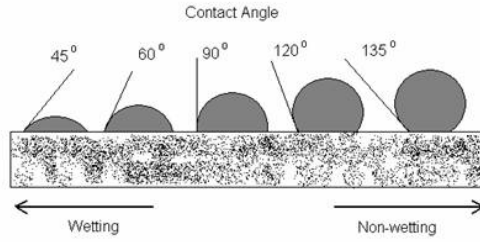


Figure 3: Distinction of phases.[13]

has specific properties which vary with pressure and temperature. In addition, a fluid can exist in different phases in the same reservoir, and also change phase with time due to variations in pressure and temperature.

For the more general case, when studying the interaction of two phases, it is common to define one phase as *wetting* and the other phase as *non-wetting*, depending on which "wets" the surface more. Figure 3 shows how the phases are distinguished. We will refer to these phases in our flow scenarios. Also, we will restrict our study to the case of *immiscible* flow, hence there is no mass transfer between the phases during flow.

3.2.2 Saturation

The pore volume fraction occupied by each phase is called the phase saturation, s_α , and the sum of all phase saturations in a pore is always equal to one. In our case,

$$s_{nw} + s_w = 1.$$

3.2.3 Capillary Pressure

When immiscible phases interact, an interfacial tension is created by the difference in phase pressure. It is called *capillary pressure*, and is defined as

$$p_c(s_\alpha) = p_{nw} - p_w. \quad (4)$$

It is usually assumed to be a function depending on phase saturations only. Hence, for a two-phase system, given one phase pressure and the saturation of that phase, the function returns the phase pressure of the *other* phase. In our case, we set the capillary pressure equal to zero, which makes the phase pressures inside the pores equal, $p_{nw} = p_w$.

3.2.4 Relative Permeability

For multiphase flow in a porous system, the flow of one phase depends on the other phases that are present at the specific pore location. Also, each phase's ability to flow will be reduced or increased as the saturation of other phases in the same location is increased or decreased. We therefore define *relative permeability*,

$$k_{r\alpha} = k_{r\alpha}(s_\alpha)$$

as a saturation dependent, dimensionless measure between 0 and 1 of how one phase will behave relative to another. The *effective* permeability for phase α is given by

$$\mathbf{K}_\alpha = \mathbf{K}k_{r\alpha}.$$

Note that the relative permeabilities are non-linear functions of saturation, and that the sum of the $k_{r\alpha}$ will not necessarily add up to 1 inside a fixed pore volume.

3.2.5 Mobility

For multiphase flow we also introduce the *mobility*, λ , of a phase. It substitutes the relation

$$\lambda_\alpha = \frac{k_{r\alpha}}{\mu_\alpha},$$

and thus simplifies our notation.

4 Continuum Mechanics

Continuum mechanics is [12] *the study of motion, kinematics and dynamics of continuous systems of particles in gases, solids and fluids*. The governing principles in continuum mechanics are the conservation laws for mass, momentum and energy. From these, the *field equations* are derived. The field equations are non-linear partial equations for unknown quantities such as density, pressure, etc. The equations are developed from the concept that the material under investigation is a continuum, and can in turn be stated in *integral* and *differential* form. Which form to choose depends on our application, whether we want to study a region or a point/particle. Both forms are equally valid and can be derived from each other for sufficiently smooth solutions.

4.1 Conservation of Mass

Assuming mass conservation in a system translates to claiming that the following equality holds:

$$\{\text{mass change in } \Omega\} + \{\text{flow in/out of } \Omega\} = \{\text{sink/source mass contribution}\}$$

for an arbitrary volume Ω . On integral form, the equality can be stated as

$$\frac{d}{dt} \int_{\Omega} \phi \rho_{\alpha} dx + \int_{\partial\Omega} (\rho \mathbf{v}) \cdot \mathbf{n} ds = \int_{\Omega} q_s dx. \quad (5)$$

The first term on the LHS is the evaluation of mass in a volume over time. The second term, which expresses the flow out of Ω , is estimated by integrating mass flux, $(\rho \mathbf{v})$ over the surface $\partial\Omega$, where \mathbf{v} is the flow velocity and n is the unit vector normal to Ω . q_s is the net mass production by sources and sinks.

We wish to have the LHS on a more manageable form, or rather, to be able to integrate all terms over the same domain. We therefore want to apply the *Divergence Theorem*, which states [5]

Divergence Theorem. *Suppose that $\partial\Omega$ is a closed, piecewise smooth surface that bounds the space region Ω . Let $\mathbf{F} = A\mathbf{i} + B\mathbf{j} + C\mathbf{k}$ be a vector field with component functions that have continuous first-order partial derivatives on Ω and \mathbf{n} be the outer unit normal vector to $\partial\Omega$. Then*

$$\iint_{\partial\Omega} \mathbf{F} \cdot \mathbf{n} dS = \iiint_{\Omega} (\nabla \cdot \mathbf{F}) dV. \quad (6)$$

We assume that our choice of \mathbf{v} satisfies these conditions, i.e. we can assume that $\rho \mathbf{v}$ is continuously differentiable over a neighbourhood of any Ω . Hence we can apply the divergence theorem to the the surface integral;

$$\int_{\partial\Omega} \rho \mathbf{v} \cdot \mathbf{n} ds = \int_{\Omega} (\nabla \cdot \rho \mathbf{v}) dx. \quad (7)$$

We put the RHS into (5),

$$\frac{d}{dt} \int_{\Omega} \phi \rho dx + \int_{\Omega} \nabla \cdot (\rho \mathbf{v}) dx = \int_{\Omega} q_s dx, \quad (8)$$

so now we can add it all up,

$$\int_{\Omega} \left(\frac{\partial}{\partial t}(\phi \rho) + \nabla \cdot (\rho \mathbf{v}) - q_s \right) dx = 0. \quad (9)$$

Furthermore, since equation (9) is valid for an arbitrary volume Ω , *du Bois-Reymond Lemma*[22] tells us that it is equally valid to consider the equation

$$\frac{\partial(\phi\rho)}{\partial t} + \nabla \cdot (\rho\mathbf{v}) = q_s, \quad (10)$$

where q_s represents the flow in or out of the system. This equation is commonly known as a *continuity* equation, and from it we can deduce more specific transport equations.

But first we need an expression for the volumetric flow velocity, \mathbf{v} .

4.2 Darcy's Law

The french engineer Henry Darcy conducted a series of experiments in the mid 1850s, investigating the durability of the Dutch dikes. In his experiments he tested how water would flow vertically through various types of sand. He discovered that no matter which type of sand he used, the fluid flow velocity, v , was always given by

$$v = \alpha \frac{\Delta p}{h},$$

where α was a constant that varied with the type of sand he used and Δp was the difference in pressure from top to bottom of dike.

His experiments has since then been repeated by the scientific community and has been subject to an extensive variation of input data. Water has been replaced by all imaginable fluids, flow has been tested in all directions and as a result we now have the empirical relation

$$v = -\frac{K}{\mu} \left(\frac{\Delta p}{L} + \rho g \cos \theta \right),$$

where K is the permeability, μ and ρ is the viscosity and density of the fluid, g is the gravity term and θ is the angle of flow direction relative to the surface normal.

We now apply this relation to an infinitesimal volume element with sides dx , dy and dz . Taking \mathbf{i} , \mathbf{j} and \mathbf{k} as unit vectors in x , y and z -directions respectively, the flow, \mathbf{v} , along the x -axis through the reference volume element(see figure 4) is described by

$$v = -\frac{K}{\mu} \left[\frac{p(x+dx) - p(x)}{dx} + \rho g \mathbf{k} \right],$$

where the last term represent the gravitational pulldown force.

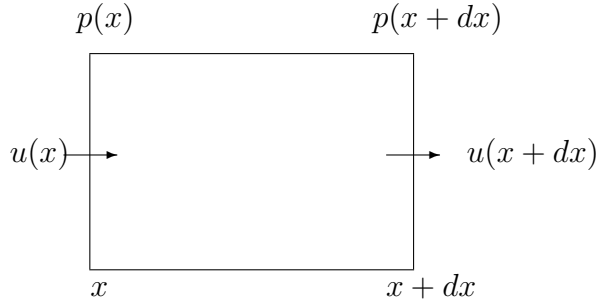


Figure 4: Darcys law on a 1D infinitesimal element

Now if we let $dx \rightarrow 0$, K, μ and ρ will not vary throughout the volume element, while

$$\frac{p(x + dx) - p(x)}{dx} \rightarrow \frac{dp}{dx}.$$

This means that

$$v(x) = -\frac{K}{\mu} \left[\frac{dp}{dx} + \rho g \mathbf{k} \right].$$

This argument is now generalised to three spatial dimensions, such that

$$\mathbf{v} = -\frac{K}{\mu} \left[\frac{\partial p}{\partial x} \mathbf{i} + \frac{\partial p}{\partial y} \mathbf{j} + \left(\frac{\partial p}{\partial z} + \rho g \right) \mathbf{k} \right],$$

or in a shorter form, which is the equation known as **Darcy's law**:

$$\mathbf{v} = -\frac{K}{\mu} [\nabla p + g\rho \nabla z]. \quad (11)$$

The processes described by this law occur when the fluid velocity, \mathbf{v} , is relatively low and the friction between the pore wall and fluid is substantial. If the fluid velocity is high or the fluid is so thin that it flows without friction, the validity of the law breaks down. These cases must be modelled by a different set of equations. However, flow velocities in porous medium is always well within the region of assumed validity of Darcy's law. Also, for sufficiently smooth ρ and p , \mathbf{v} from (11) satisfies the conditions of the Divergence theorem, hence we use \mathbf{v} to express our flow velocity.

4.3 Two-Phase Flow

The equations that govern two phase flow are the same conservative equations as we deduced for the single phase case, but now we also include the multiphase variables and functions from section 3.2.

The sum of all phases present in a pore is equal to one, $\sum_{\alpha} s_{\alpha} = 1$, and a multiphase equation can be expressed intuitively as the sum

$$\frac{\partial}{\partial t} \left(\phi \sum_{\alpha} \rho_{\alpha} s_{\alpha} \right) + \nabla \cdot \left(\sum_{\alpha} \rho_{\alpha} v_{\alpha} \right) = \sum_{\alpha} q_{\alpha}. \quad (12)$$

Our approach is rather to couple the equations by inserting the saturation relation, $s_w = 1 - s_{nw}$, and solve the two phase equations individually;

$$\frac{\partial}{\partial t} (\phi \rho_w (1 - s_{nw})) + \nabla \cdot \rho_w v_w = q_w, \quad (13)$$

$$\frac{\partial}{\partial t} (\phi \rho_{nw} s_{nw}) + \nabla \cdot \rho_{nw} v_{nw} = q_{nw}, \quad (14)$$

We use Darcy's law to express phase flow velocities,

$$v_{\alpha} = -\mathbf{K} \frac{k_{r\alpha}}{\mu_{\alpha}} (\nabla p + g \rho_{\alpha} \nabla z), \quad \alpha = w, nw \quad (15)$$

where we have introduced the relative permeability term, k_r , to balance the reduced flow ability of the phases present in the pore. We have also now included that the capillary pressure is set to 0, meaning that the pressure gradient is the same for both phase velocities.

In some cases it is convenient to consider a simplified version. From section 3.1.6, we know that when assuming incompressible flow, we consider phase density as constant and set the rock porosity to not change over time. The temporal differential term then vanishes, and equation (10) for phase α becomes

$$\nabla \cdot (\rho_{\alpha} v_{\alpha}) = q_{\alpha}. \quad (16)$$

or, equivalently,

$$\nabla \cdot v_{\alpha} = \frac{q_{\alpha}}{\rho_{\alpha}} \quad (17)$$

Expressions on this form describe the flow of fluids independent of time. However, all fluids are compressible to some extent, and we add this property to our expression.

Compressibility

For a compressible fluid, density changes with pressure and temperature. In mathematical terms, we say that the density, ρ , of phase α is a function of pressure and temperature,

$$\rho_\alpha = \rho_\alpha(p, T),$$

and the temporal change is expressed as partial derivatives of ρ_α with respect to these variables,

$$\frac{\partial \rho_\alpha}{\partial t} = \frac{\partial \rho_\alpha}{\partial p_\alpha} \frac{\partial p_\alpha}{\partial t} + \frac{\partial \rho_\alpha}{\partial T_\alpha} \frac{\partial T_\alpha}{\partial t}. \quad (18)$$

We want to include the compressibility and thermal expansion coefficients from sections 3.1.4 and 3.1.5 in the continuity equation for phase α

$$\frac{\partial}{\partial t}(\phi \rho_\alpha s_\alpha) + \nabla \cdot (\rho_\alpha v_\alpha) = q_\alpha. \quad (19)$$

By reformulating them, we get

$$\frac{\partial \rho_\alpha}{\partial p_\alpha} = c_\alpha \rho_\alpha, \quad \frac{\partial \rho_\alpha}{\partial T_\alpha} = -\beta_\alpha \rho_\alpha$$

which we insert in (18), and get

$$\frac{\partial \rho_\alpha}{\partial t} = \rho_\alpha \left(c_\alpha \frac{\partial p_\alpha}{\partial t} - \beta_\alpha \frac{\partial T_\alpha}{\partial t} \right). \quad (20)$$

In addition, since the reservoir porosity ϕ is a function of overall reservoir pressure, p , we must also include the *rock* compressibility, c_r , which is defined in an equivalent manner as c_α ,

$$c_r = \frac{1}{\phi} \frac{\partial \phi}{\partial p},$$

To fit dependency this into our expression, we utilize that

$$\frac{\partial \phi}{\partial t} = \frac{\partial \phi}{\partial p} \frac{\partial p}{\partial t} = c_r \phi \frac{\partial p}{\partial t} \quad (21)$$

By inserting the above expressions into equation (19), we get the following expression for compressible flow of phase α

$$s_\alpha c_r \phi \frac{\partial p}{\partial t} + \phi s_\alpha \left(c_\alpha \frac{\partial p_\alpha}{\partial t} - \beta_\alpha \frac{\partial T_\alpha}{\partial t} \right) + \phi \frac{\partial s_\alpha}{\partial t} + \nabla \cdot (\rho_\alpha v_\alpha) = \frac{q_\alpha}{\rho_\alpha}. \quad (22)$$

Another common way of solving the set of equations, is to set up pressure and transport equations based on the multiphase equation, summing up the mass conservation equations for all phases. An outline of the pressure equation deduction is included in Appendix B.

5 Thermal Flow

In order to investigate the geothermal energy recovery potential in a system, we need to model flow as non-isothermal. Thus we must extend our set of equations to also incorporate the thermal flow. We deduce this expression from the principle of energy conservation much in the same manner as the phase continuity equations are deduced from the principle mass conservation. One important difference is that for the equations of mass conservation, the matrix itself does not transmit any particles. For energy conservation, however, we have to consider heat conduction through the matrix, interpreted as flow. We do this by adding an expression for point-wise evaluation of the system temperature. But first we need to define some key concepts.

5.1 Energy, Heat and Work

In thermodynamics, the two main mechanisms that are able to transfer internal energy U are *work* and *heat*.

Heat is defined as [21] any spontaneous flow of energy from one object to another caused by a difference in temperature between the objects. As in the case for motion of fluids, we say that heat *flows*. It is represented by the letter Q in our equations.

Work is in thermodynamics any other action that causes the transfer of energy into or out of a system in a time period. It is a process that for instance increases the system temperature. We use W to denote work.

The three concepts energy, work and heat are connected through the *First Law of Thermodynamics*. It concerns the conservation of energy and simply states that *energy can neither be created nor destroyed*.

Heat and work as above refer to energy in transit, one does not deal with the work/heat *in* a system. If a system undergoes a process by heat and work, then the net heat supplied, Q , plus the net work done, W , is equal to the change of internal energy, U , of the fluid or solid between states 1 and 2,

$$U_2 - U_1 = \Delta U = Q + W. \quad (23)$$

The SI unit of Energy is *Joule*, and is defined as kgm^2/s^2 .

5.2 Heat Transfer

Heat transfer processes are classified into the categories *conduction*, *convection* and *radiation*. The two first categories are defined below. Radiation is primarily related to heat transfer through emission of electromagnetic waves, and thus not relevant for our model.

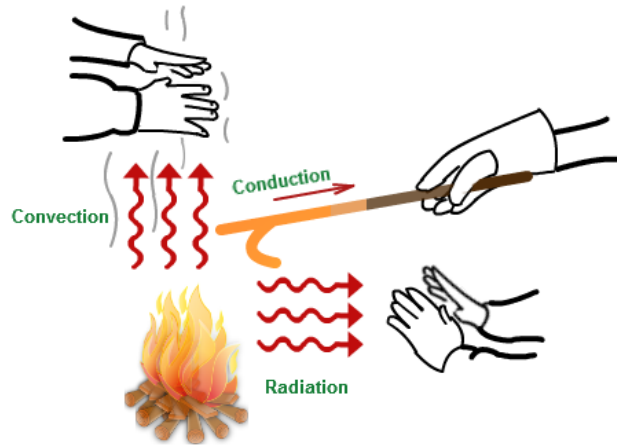


Figure 5: Three processes of heat transfer

5.2.1 Conduction

Conduction of heat is the transfer of energy through molecular diffusion, i.e. via direct contact at molecular level. In a fluid or gas phase, the transfer happens when fast molecules *collide* with slower molecules, whilst between non-metallic solids, heat is conducted via grouped particle *vibration*. The average energy per molecule is a function of temperature, and the flux, q_c , is governed by Fourier's (empirical) law of heat conduction. In analogy with Darcy's law for fluids, it states that flow occurs from an area of high temperature to an area of low temperature,

$$q_c = -k_T \nabla T. \quad (24)$$

where ∇T is the temperature gradient, and k_T is the thermal conductivity coefficient. k_T is a measure of a material's ability to conduct heat and the corresponding unit is W/mK.

5.2.2 Convection

Convection is the type of heat transfer which one intuitively would associate with moving fluids. It is the collective movement of particles within fluids, but we must also take into account the result of random local molecular motion. Convection is therefore divided into two separate processes, it occurs either through *diffusion*, *advection* or as a combination of both.

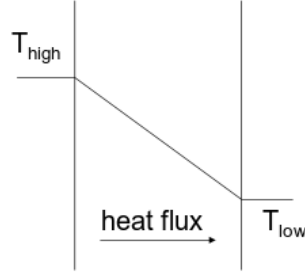


Figure 6: Fourier's law of conduction

Diffusion

Diffusion is caused by a difference in the concentration, n , of particles, N , in a sample volume V ,

$$n = \frac{N}{V}. \quad (25)$$

The flux density, J_{diff} , of these particles is estimated much in the same manner as Fourier's law of conduction, using Fick's Law,

$$J_{diff} = -D\nabla n, \quad (26)$$

where D is the diffusion coefficient. D depends both on the molecule type that is diffusing and what it is diffusing through.

Advection

Advection occurs when a fluid moves and by this transports some inherent property, in our case heat. This type of heat transfer is called *advective flux*. The advective flux density is expressed through the concentration of the property and the flow velocity;

$$J_{adv} = nv. \quad (27)$$

5.3 Specific Heat Capacity

The heat capacity, C , of an object is the amount of heat required to raise the temperature, per degree temperature increase,

$$C = \frac{Q}{\Delta T}. \quad (28)$$

It is thus quite loosely defined, a more fundamental quality is the *Specific Heat Capacity*, which is the amount of heat required to raise the temperature of a *unit mass* of an object by one unit;

$$c = \frac{C}{m} = \frac{Q}{m\Delta T}. \quad (29)$$

It is usually denoted c , and expressed in units of Joules per Kilogram Kelvin.

Since the temperature of a system can be raised in many ways, we need to specify in which manner we choose to evaluate the system. In our model we will use heat capacities $c_{p\alpha}$ and $c_{V\alpha}$ which represent the specific heat capacities of phase α at constant *pressure* and constant *volume*. The specific heat capacities for rock, in order to avoid any confusion with the compressibility factor c_r , will be named κ_r .

5.4 Entropy

The second law of thermodynamics introduces the concept of *entropy*, S , of a system. It states that [1] "The entropy of the universe is increased through all real processes", which translates to $\Delta_{Total}S \geq 0$. Entropy is defined using statistical physics, but we can gain an understanding of it by observing how it changes; if an amount of heat ΔQ is introduced into a system at an absolute temperature, T , the increase of the system entropy is expressed as

$$\Delta S = \frac{\Delta Q}{T}. \quad (30)$$

5.5 Internal Energy

The internal energy of a system can be described as the energy involving the motion on the molecular level, the energy of the system due to its thermodynamic properties such as pressure and temperature.

It is not possible to measure this energy directly, but one can determine the internal energy of a system through a chain of thermodynamic processes involving the use of empirical data. Such a chain can be theoretically described by the system state variables, i.e. entropy, S , volume, V , etc.. The internal energy, U , is a function of those, $U(S, V, \dots)$.

Specific Internal Energy

The variable used in our equation is the *specific internal energy*, u , and is defined as the internal energy of the system *per unit mass*.

$$u = \frac{U}{m}.$$

5.6 Enthalpy

The most convenient way to define enthalpy, H , of a system is through the relation

$$H = U + pV, \quad (31)$$

where U is the energy, p is the pressure and V is the volume of the system. It is an expression of the *total energy* you would be left with after adding the work that is necessary to annihilate the system. The work that is required to do so must be added to the original amount of energy in the system. This work is done by pV , which is the pressure from the environment times the volume of the system.

Specific Enthalpy

The specific enthalpy equals the energy and the energy that is transferred to the environment through the expansion of the system;

$$h = \frac{H}{m} = \frac{U + pV}{m} = u + \frac{p}{\rho}. \quad (32)$$

In our energy equations, we will use the phase specific internal energy u_α and the specific enthalpy h_α . These can be computed from

$$u_\alpha = c_{V\alpha}T,$$

$$h_\alpha = c_{p\alpha}T,$$

where $c_{V\alpha}$ and $c_{p\alpha}$ are as defined above. It is also possible to deduce one from the other by the relation

$$h_\alpha = u_\alpha + \frac{p_\alpha}{\rho_\alpha}.$$

5.7 Energy Equation

The principle of the conservation of energy can be formulated as the equality [10]

$$\{\text{Rate of energy production in } \Omega\} + \{\text{Net rate of energy transported into or out of } \Omega\} = \{\text{Rate of accumulation of energy in } \Omega\}$$

where Ω is an arbitrary volume as in section 4.1. On integral form, the equality translates to

$$\frac{\partial}{\partial t} \int_{\Omega} (\rho_t U) dx + \int_{\partial\Omega} E \cdot \mathbf{n} ds = \int_{\Omega} W dx \quad (33)$$

where $\rho_t U, E$ and W represent energy concentration, flux and source, respectively. U is an overall internal energy and ρ_t is an overall density.

Since we are in modelling flow in a porous medium, flow velocities are small and we disregard the contributions from kinetic energy. In addition, the energy flux contributed by radiation will be neglected. By applying the divergence theorem to the flux term, we can rewrite equation (33) as

$$\int_{\Omega} \frac{\partial}{\partial t} (\rho_t U) + \nabla \cdot E - W \, dx = 0. \quad (34)$$

The overall density ρ_t is a sum of phase and rock densities,

$$\rho_t = \phi \sum_{\alpha} \rho_{\alpha} s_{\alpha} + (1 - \phi) \rho_r,$$

and the total internal energy is thus defined as

$$\rho_t U = \phi \sum_{\alpha} \rho_{\alpha} s_{\alpha} u_{\alpha} + (1 - \phi) \rho_r \kappa_r T, \quad (35)$$

where u_{α} is the specific internal energy per unit mass of phase α , whilst κ_r and ρ_r is the specific heat capacity and density of the rock. Energy flux, E , is made up of convective contributions from the flowing phases and heat conduction from rock,

$$E = \left(\sum_{\alpha} \rho_{\alpha} v_{\alpha} u_{\alpha} \right) + q_c, \quad (36)$$

where the convective term is as defined in section 5.2.2 and q_c is the conductive flux, defined in section 5.2.1 as Fourier's law of conduction

$$q_c = -k_T \nabla T. \quad (37)$$

As before, k_T is the rock conductivity coefficient and T the temperature of the control volume.

To simplify the equation, we assume that the system is in *local thermal equilibrium*. This means that although temperature varies in time and space throughout Ω , we assume that it varies very slowly. Hence, in a control volume, Ω_i , and in a neighbourhood around it, all present phases have the same temperature, T .

For the source term, W , we regard it as a sum

$$W = W_{pV} + W_g,$$

where the terms represent rate of work against a pressure field and gravity, respectively, and is expressed by

$$W = - \sum_{\alpha} \nabla \cdot (p_{\alpha} v_{\alpha}) - \rho_{\alpha} v_{\alpha} \cdot g \nabla z, \quad (38)$$

where v_{α} is the Darcy velocity as for the mass conservation . Inserting equations (35)-(38) into (34) and applying the same argumentation as in the transition from equation (9) to equation (10), the energy conservation equation becomes

$$\begin{aligned} \frac{\partial}{\partial t} \left(\phi \sum_{\alpha} \rho_{\alpha} s_{\alpha} u_{\alpha} + (1 - \phi) \rho_r \kappa_r T \right) + \nabla \cdot \sum_{\alpha} \rho_{\alpha} v_{\alpha} u_{\alpha} \\ - \nabla \cdot (k_T \nabla T) + \sum_{\alpha} (\nabla \cdot (p_{\alpha} v_{\alpha}) - \rho_{\alpha} v_{\alpha} \cdot g \nabla z) = 0. \end{aligned} \quad (39)$$

For the divergence spatial terms, we introduce the specific enthalpy, h_{α} from section 5.6,

$$h_{\alpha} = u_{\alpha} + \frac{p_{\alpha}}{\rho_{\alpha}}.$$

This allows us to express p_{α} as

$$p_{\alpha} = \rho_{\alpha} (h_{\alpha} - u_{\alpha}), \quad (40)$$

and thus by replacing p_{α} in the pressure-volume work term in (39), we eliminate u_{α} from the divergence terms, resulting in

$$\begin{aligned} \frac{\partial}{\partial t} \left(\phi \sum_{\alpha=w}^g \rho_{\alpha} s_{\alpha} u_{\alpha} + (1 - \phi) \rho_r \kappa_r T \right) + \nabla \cdot \sum_{\alpha} (\rho_{\alpha} v_{\alpha} h_{\alpha}) \\ - \nabla \cdot (k_T \nabla T) - \sum_{\alpha} \rho_{\alpha} v_{\alpha} \cdot g \nabla z = 0. \end{aligned} \quad (41)$$

Finally, we disregard the the effect of gravitational forces, as the effect on thermal energy from gravity is negligible. Our multiphase expression for energy conservation then becomes

$$\frac{\partial}{\partial t} \left(\phi \sum_{\alpha} \rho_{\alpha} s_{\alpha} u_{\alpha} + (1 - \phi) \rho_r e_r \right) + \nabla \cdot \left(\sum_{\alpha} (\rho_{\alpha} v_{\alpha} h_{\alpha}) - k_T \nabla T \right) = 0, \quad (42)$$

where

$$e_r = \kappa_r T. \quad (43)$$

Formation Volume Factor

Ideally we would like to study a system of equations where the unknown variables are evaluated under equal conditions. A common approach is to include a dimensionless factor named *formation volume factor* B_α , which determine the volume relation between phase conditions. In the terminology of the oil industry, the known factor is a constant indexed by *STC*, *stock tank conditions*, and the variable factor is indexed by *RC*, or *reservoir conditions*,

$$B_\alpha = \frac{V_\alpha(RC)}{V_\alpha(STC)}.$$

Since mass does not change between RC and STC, the volumes V_α can be replaced by the respective densities, ρ_α .

$$B_\alpha = \frac{\rho_\alpha(STC)}{\rho_\alpha(RC)}.$$

The formation volume factors will thus replace the density variable in our equations. Furthermore, it is common practice to use the *inverse* volume factors, $b_\alpha = 1/B_\alpha$. We will apply this notation and also put it in a more compact form, hence we define

$$\rho_\alpha = \rho_{\alpha S} b_\alpha. \quad (44)$$

5.8 Final Set of Equations

Conservation of mass

We insert the new expression for ρ_α into our equation

$$\frac{\partial(\phi \rho_{\alpha S} b_\alpha s_\alpha)}{\partial t} + \nabla \cdot (\rho_{\alpha S} b_\alpha v_\alpha) = q_\alpha, \quad (45)$$

since $\rho_{\alpha S}$ is a constant and divergence is a linear operator, we arrive at the following two equations of mass conservation;

$$\frac{\partial(\phi b_w s_w)}{\partial t} + \nabla \cdot (b_w v_w) = \frac{q_w}{\rho_w S}, \quad (46)$$

$$\frac{\partial(\phi b_{nw} s_{nw})}{\partial t} + \nabla \cdot (b_{nw} v_{nw}) = \frac{q_{nw}}{\rho_{nw} S}, \quad (47)$$

where the volumetric flow velocity is represented the Darcy flow velocity

$$v_\alpha = -\mathbf{K} \frac{k_{r\alpha}}{\mu_\alpha} (\nabla p - g \rho_{\alpha S} b_\alpha \nabla z) \quad (48)$$

for wetting and non-wetting phases α , $b_\alpha(p)$ is the phase volume formation factor and s_α is the phase saturation.

Conservation of energy

The conservation of energy is governed by a set of equations combining fluid and rock properties.

$$\sum_{\alpha} \left(\frac{\partial(\phi b_{\alpha} u_{\alpha} s_{\alpha})}{\partial t} + (\nabla \cdot (b_{\alpha} h_{\alpha} v_{\alpha})) \right) + \frac{\partial(1 - \phi) e_r}{\partial t} - \nabla \cdot (k_T \nabla T) = 0, \quad (49)$$

where v_{α} is the Darcy velocity from (48),

$$u_{\alpha} = c_{V\alpha} T, \quad h_{\alpha} = c_{p\alpha} T,$$

where $c_{V\alpha}$ is the volumetric heat capacity and $c_{p\alpha}$ the fluid heat capacity under constant pressure, both given as scalars. In the same manner,

$$e_r = \kappa_r T.$$

6 Fractures

Equivalent to what we stated about porosity, all rock in the earth's crust are fractured to some extent. Fractures occur as a response to stress, and the source of this stress can be from various processes. It can stem from the sheer weight of the earth's crust, tectonic forces, fluid pressure or be a result of thermal activity.

Fractures affect many aspects of reservoir mechanics, by providing pathways for fluid flow or creating barriers that prevent flow across them. They also have an impact on the stability of structures. Since many petroleum, gas, geothermal, and water supply reservoirs form in fractured rocks, the understanding of fracture behaviour and flow in these is of importance in geo-technical engineering and thus in reservoir simulation.

6.1 Fracture Models

Several conceptual models have been developed for describing fluid flow in fractured porous media. The methods differ in how they model storage and flow capabilities of the porous medium and the fracture. The storage characteristics are associated with porosity, and the flow characteristics are associated with permeability. In our model, we have chosen to look at flow in fractures where permeability of the matrix is very low. Conceptually, this type of geology is modelled by the Discrete Fracture Network model. However, the DFN model is based on a Dual-Continuum Formulation model which we define below.

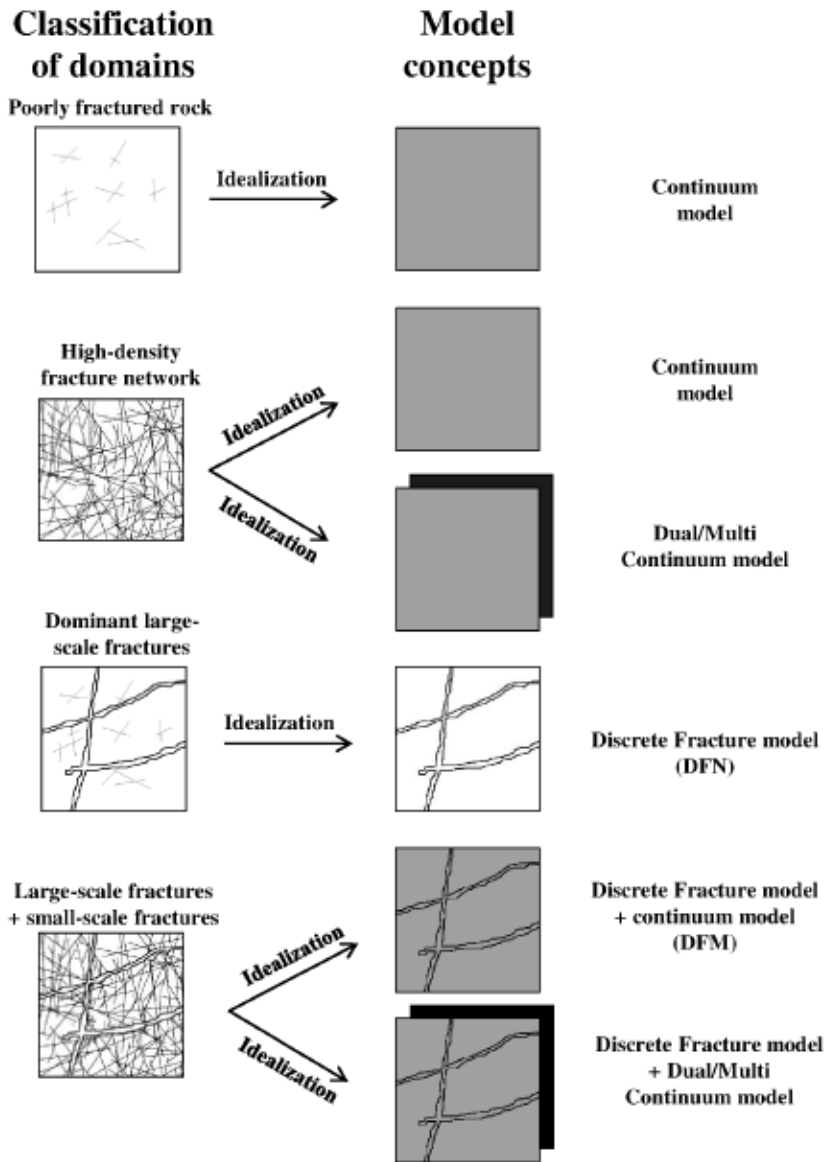


Figure 7: Macro Scale modeling concepts(Sandve 2012)

Dual-Continuum Formulation model

A Dual-continuum model depicts an idealized flow medium with two different values of porosity, the primary is created by deposition, the second by fracturing or dissolution. This distinction leads to a division of the medium in two separate parts, matrix and fractures. The weighting is set to regard unfractured rock to have much of the the storage of the medium, but little of the flow. Conversely, fractures may have negligible storage ability, but high permeability. The porous medium and the fractures are seen as two separate but overlapping continua.

Discrete Fracture Model

In a Dual Continuum model, fluid mass transfers between porous media and fractures over interfaces. In short, discrete fracture network models describe a type of dual-continuum models in which the permeability is so low that almost all fluid flow is restricted to the fractures. Heat, however, is transmitted between the matrix and fracture cells.

6.2 Flow in Fractures

Flow in fractures differ slightly from flow in a porous medium. The fracture *aperture* is the perpendicular height of an open fracture. It is however difficult to truly determine the fracture aperture within a rock body. In our model, we consider the flow between two parallel plates of constant aperture, h and width, w . Since the volume between the plates is open and not a porous medium, the volumetric flow velocity over adjacent control volume surfaces is governed by a different set of equations. For modelling viscous flow, we can begin with Navier Stokes equations;

$$\rho_{\alpha} \left(\frac{\partial \mathbf{u}}{\partial t} + \mathbf{u} \cdot \nabla \mathbf{u} \right) = -\nabla p + \mu \nabla^2 \mathbf{u}. \quad (50)$$

Fracture permeability is generally defined under the assumption of steady-state flow, i.e $\frac{\partial \mathbf{v}}{\partial t} = 0$. Assuming this and *no-slip* boundary conditions, which specify that at any boundary between the fluid and a solid, the velocity vector of the fluid must be equal to that of the solid. This implies that at the fracture walls, not only the normal component of the velocity equals to zero, but the tangential component vanishes as well. Hence for fracture flow, we evaluate the linear Stokes equation;

$$\nabla p = \mu \nabla^2 \mathbf{u}. \quad (51)$$

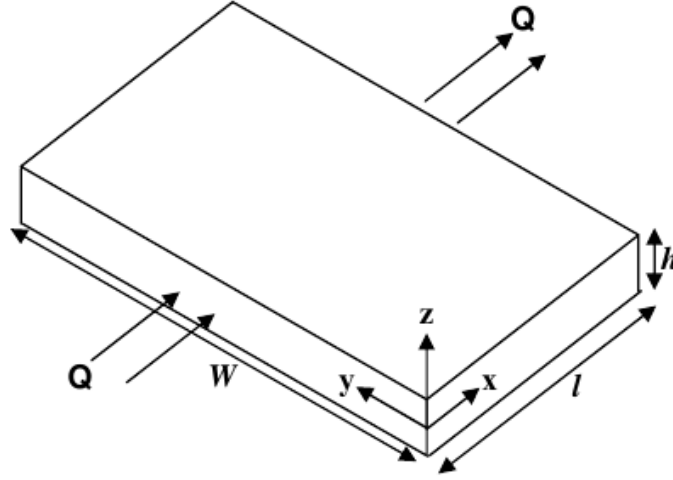


Figure 8: Flow between parallel plates (Sarkar E.T.)

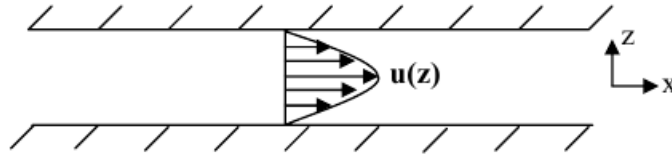


Figure 9: Velocity profile (Sarkar E.T.)

In addition, we assume that the pressure at the inlet, p_1 is greater than the pressure at the outlet, p_2 . Linearising the negative gradient, equation (50) is reduced to

$$\frac{p_1 - p_2}{l} + \mu \nabla^2 \mathbf{u} = 0 \quad (52)$$

The flow is in the x -direction, therefore only the x -component of the velocity, $u_x(z)$, exists. Integrating this equation twice w.r.t. z and inserting the boundary conditions $u_x(0) = u_x(h) = 0$ gives us the velocity profile (figure 9)

$$u_x(z) = \frac{1}{2\mu} \frac{p_1 - p_2}{l} z(h - z). \quad (53)$$

By integrating $u_x(z)$ over $[0, h]$ and multiplying by the width, W , we get an expression for the *volumetric flow rate* in x -direction,

$$Q_{V_x} = \frac{Wh^3}{12\mu} \frac{(p_1 - p_2)}{l}. \quad (54)$$

Furthermore, the *average flow velocity*, \bar{u} can be estimated by dividing Q_{V_x} by the cross-sectional area of the fracture, Wh

$$\bar{u} = \frac{Q_{V_x}}{Wh} = \frac{h^2}{12\mu} \frac{(p_1 - p_2)}{l} \quad (55)$$

which makes \bar{u} equivalent to the Darcy velocity for flow in porous medium with a medium permeability $\mathbf{K} = h^2/12$. Thus we conclude that we are able to estimate flow in *fractured* porous media by adjusting only the permeability factor in the equations that govern flow over the control volumes which represent fractures.

The representation of fractures as cubic voids between smooth parallel plates as above, is of course a strong simplification of how fractures occur and influence flow in a reservoir. In nature, the fracture permeability is anything but constant. We will not pursue this matter in our model, but the MRST tools applied in the experiments section are able to handle this type of permeability input.

Two-Phase flow in fractures

We will be modelling a reservoir where the fractures are fully saturated by a composition of phases. For single-phase flow, fracture geometry at the aperture scale governs the fluid flow and transport properties. When we have two-phase immiscible fluid flow conditions, the aperture each phase experiences is a product of the phase geometry in the fracture. This effects the relative permeability and therefore fluid pressure/saturation relation. In addition, this phase geometry also influences flow and transport into and through the surrounding porous matrix blocks. In our work, however, we will be using the DFN model, in which the effects of fluid flow between fractures and matrix are not considered.

7 Numerics

Background

The conservation equations derived above govern the flow of mass and energy in time and space in a quite intuitive manner. We now seek to evaluate these under different initial and boundary conditions to help us predict the behaviour of the system over time. To do so, we must solve a set of partial differential equations, or PDEs, which ideally returns a function. However, solving this set of equations analytically is a tedious task, and practically impossible when the problems are large (and nonlinear). Therefore, a numerical

approximation of the time and space derivatives in the PDE is performed. Instead of evaluating the differential operator continuously, we split the time scale into discrete steps and evaluate the difference between values at points. We take the PDE from a continuous setting into a discrete setting by performing a discretization, which makes us able to solve the approximated PDE on a computer using an iterative method.

The discretisation in time and space require different approaches. For the spatial operators, we will be using a finite volume method called two point flux approximation and a method that determines values based on the direction of the flux called the *upstream* method. For the temporal term, we use an implicit finite difference method, the backward Euler.

7.1 Spatial Discretisation

7.1.1 Finite Volume Methods

Finite Element and Finite Volume methods are based on an *integral formulation* of the PDE. The domain Ω is represented and structured by a grid, and the grid cells, Ω_i represents *control volumes*. After applying the divergence theorem, which converts any divergence term to a boundary flux term, the PDE is replaced by a balance equation which represents flux over adjacent grid cell faces. The set of these balance equations is then discretised, and the PDE is solved over Ω in an averaged sense.

What distinguishes Finite Volume Methods from Finite Difference Methods, is that the discretisation is performed on local balance equations, rather than the original PDE. The fluxes on the control volume boundaries, rather than the differential operator, are discretised.

The resulting system of discrete equations depends on a finite set of unknowns, and may be either linear or non linear, depending on the PDE and boundary conditions. This system is then solved approximately, using for example direct or iterative solvers in the case of linear equations and fixed point or Newton type methods in the case of nonlinear equations.

As an example, we apply FVM to the continuity equation for phase w , hence moving "backwards" from the procedure in 4.1,

$$\frac{\partial(\phi\rho_w)}{\partial t} + \nabla \cdot (\rho_w v_w) = q_s. \quad (56)$$

Assuming porosity does not change over time and density is constant, the temporal term vanishes so we only look at

$$\nabla \cdot v = \frac{q}{\rho}, \quad (57)$$

v is the Darcy flow velocity,

$$v = -\frac{\mathbf{K}}{\mu}(\nabla p - g\rho\nabla z). \quad (58)$$

The gravity term is now measured as depth, not height, and has thus changed sign. However, since we are only interested in demonstrating the appliance of finite volume methods for solving a PDE, we neglect the gravity term from here on. The flux, v , then becomes

$$v = -\frac{\mathbf{K}}{\mu}\nabla p. \quad (59)$$

Integrating equation (57) over a control volume, Ω_i , gives

$$\int_{\Omega_i} \left(\frac{q}{\rho} - \nabla \cdot v \right) dx = 0. \quad (60)$$

Assuming then that v satisfies the differentiability conditions of the divergence theorem, we get the mass-balance equation

$$\int_{\partial\Omega_i} v \cdot \mathbf{n} \, d\nu = \int_{\Omega_i} \frac{q}{\rho} \, dx, \quad (61)$$

where \mathbf{n} is the outward facing unit normal on Ω_i .

After having done this work on a PDE, one must choose which Finite Volume method to apply. In our model we have used the Two Point Flux Approximation, which is outlined below.

TPFA

The basic idea behind TPFA is to look at two adjacent cells, i , j , and by using the two averaged constant cell values estimate the flux v_{ij} over the surface between them. The procedure is then repeated for all cells j that have a common surface with cell i before moving to the next cell.

We consider a control volume, Ω_i , which is placed in a three dimensional grid with orthogonal axis in regular coordinate directions. γ_{ij} represents the surface between it and its adjacent cells in all axis orientations. For the Darcy velocity, v , we state the flux over the defined surface as

$$v_{ij} = \int_{\gamma_{ij}} v \cdot \mathbf{n} \, ds = - \int_{\gamma_{ij}} \frac{\mathbf{K}}{\mu} \nabla p \cdot \mathbf{n} \, ds, \quad (62)$$

where \mathbf{n} is the outward facing vector normal to the surface. We will consider flux in x-direction, so $\mathbf{n} = [1, 0, 0]^T$. The TPFA method approximates the

flux using two points. Generally, the gradient operator is then approximated using a central difference method,

$$\nabla p_{ij} \simeq \delta p_{ij} = \frac{(p_j - p_i)}{(c_{ij} - c_i) + (c_j - c_{ij})}, \quad (63)$$

where c is the cell and surface center. In our case, the control volumes are equally sized in an orthogonal grid, so the central difference approximation becomes

$$\delta p_{ij} = \frac{2(p_j - p_i)}{\Delta x_i + \Delta x_j} \quad (64)$$

where p_i and p_j are cell-averaged values of pressure, Δx_i and Δx_j are the cell dimensions in respective (now x -) directions, and express the distance from the respective cell centers to the surface γ_{ij} . The flux is now defined as an approximation

$$v_{ij} \simeq -\delta p_{ij} \int_{\gamma_{ij}} \frac{\mathbf{K}}{\mu} ds \quad (65)$$

In order to integrate the remainder over the surface γ_{ij} , we need its components to be well-defined on it. For thermal flow, $\mu = \mu(p, T)$, so we must find an estimate to the value over the surface. To do this we will later apply the upstream method, which will be discussed in section 7.1.2. For now, since we are only aiming to demonstrate the TPF method, we consider μ as constant over Ω . This means $\mu_{ij} = \mu_i = \mu_j$ for all cells i, j .

If the permeability tensor \mathbf{K} is set as cellwise constant, the TPF method uses a directional harmonic averaging of adjacent cell permeability values. The n_{ij} -directional permeability \mathbf{K}_{ij} is then evaluated by [1]

$$\mathbf{K}_{ij} = (\Delta x_i + \Delta x_j) \left(\frac{\Delta x_i}{\mathbf{K}_{i,ij}} + \frac{\Delta x_j}{\mathbf{K}_{j,ij}} \right)^{-1}, \quad (66)$$

where $\mathbf{K}_{i,ij} = \mathbf{n}_{ij} \cdot \mathbf{K}_i \mathbf{n}_{ij}$ and $\mathbf{K}_{j,ij} = \mathbf{n}_{ij} \cdot \mathbf{K}_j \mathbf{n}_{ij}$. Inserting this and integrating over the surface, we have an expression for the approximated flux, v_{ij} ,

$$v_{ij} \simeq -\delta p_{ij} \frac{\mathbf{K}_{ij}}{\mu_{ij}} \int_{\gamma_{ij}} ds = -|\gamma_{ij}| \delta p_{ij} \frac{\mathbf{K}_{ij}}{\mu_{ij}}, \quad (67)$$

where $|\gamma_{ij}|$ is the surface area. For an element, i , we can sum over all neighbouring cellfaces and get a discrete approximation of the LHS of (61),

$$\int_{\partial\Omega_i} v \cdot \mathbf{n} d\nu = \sum_j v_{ij} \simeq \sum_j -|\gamma_{ij}| \delta p_{ij} \frac{\mathbf{K}_{ij}}{\mu_{ij}} = \sum_j 2 \frac{|\gamma_{ij}|}{\mu_{ij}} (p_i - p_j) \left(\frac{\Delta x_i}{\mathbf{K}_{i,ij}} + \frac{\Delta x_j}{\mathbf{K}_{j,ij}} \right)^{-1}. \quad (68)$$

Transmissibilities

Terms that do not include cell averaged values are called grid *transmissibilities*, t_{ij} . They are usually evaluated initially over the grid structure and stored as a vector. For the transmissibilities in the method above we write

$$t_{ij} = 2|\gamma_{ij}| \left(\frac{\Delta x_i}{\mathbf{K}_{i,ij}} + \frac{\Delta x_j}{\mathbf{K}_{j,ij}} \right)^{-1}.$$

Inserting this in the equations above, we get

$$\sum_j \frac{t_{ij}}{\mu_{ij}} (p_i - p_j) = \int_{\Omega_i} \frac{q}{\rho} dx, \quad \forall \Omega_i \subset \Omega. \quad (69)$$

The TPFA scheme is monotone, robust and simple to implement and is therefore the industry standard.

7.1.2 Upstream Method

For operators that are hyperbolic of nature, as when involving propagation of matter, it is insufficient to use their averaged cell values. For hyperbolic terms, we evaluate the direction of the flux, v_α and choose the value *upstream*. As before, we consider the surface flux of phase α

$$v_{\alpha ij} = \int_{\gamma_{ij}} v_\alpha \cdot \mathbf{n} ds. \quad (70)$$

The upstream method for deciding an arbitrary cell value, y , then becomes

$$y_{\alpha ij} = \begin{cases} y_{\alpha i} & \text{if } v_{\alpha ij} \geq 0 \\ y_{\alpha j} & \text{if } v_{\alpha ij} < 0. \end{cases} \quad (71)$$

As an example, we consider the mobility term λ_α in a FVM. When integrating the flux over the surface γ_{ij} , the mobility term on the surface is decided by

$$\lambda_{\alpha ij} = \begin{cases} \lambda_{\alpha i} & \text{if } v_{\alpha ij} \geq 0 \\ \lambda_{\alpha j} & \text{if } v_{\alpha ij} < 0. \end{cases} \quad (72)$$

Boundary Conditions

In order to solve a PDE uniquely, we need to add some additional conditions to the system. For the spatial terms on $\partial\Omega$, we impose the *Dirichlet* and *Neumann* boundary conditions. The Dirichlet condition specifies the values

that a solution, u , needs to take on the boundary of the domain, defined as the *Dirichlet boundary*, $\partial\Omega_D$;

$$u = u_D, \quad \text{on } \partial\Omega_D \quad (73)$$

The Neumann boundary conditions specifies the values that the derivative of a solution, ∇u , is to take *over* the *Neumann boundary* $\partial\Omega_N$, hence

$$\nabla u \cdot \mathbf{n} = q_N, \quad \text{on } \partial\Omega_N \quad (74)$$

For every part of the boundary we have either a Dirichlet or Neumann condition.

7.2 Temporal Discretisation

7.2.1 Finite Difference Methods

For the temporal term, we approximate the differential operator using finite difference methods. Since all of our equations have terms involving both the differential of time and space, the scheme outlined below applies to both the mass and energy conservation equations. We consider two coupled PDEs

$$\frac{\partial}{\partial t} \int_{\Omega_i} g_w dx = \int_{\Omega_i} F(g_w, g_{nw}) dx, \quad (75)$$

$$\frac{\partial}{\partial t} \int_{\Omega_i} g_{nw} dx = \int_{\Omega_i} G(g_w, g_{nw}) dx, \quad (76)$$

where F,G are spatial terms. When dividing both sides by the volume of cell i , we get the average integral value on both sides (for cell i),

$$\frac{\partial}{\partial t} \frac{1}{|\Omega_i|} \int_{\Omega_i} g_w dx = \frac{1}{|\Omega_i|} \int_{\Omega_i} F(g_w, g_{nw}) dx, \quad (77)$$

$$\frac{\partial}{\partial t} \frac{1}{|\Omega_i|} \int_{\Omega_i} g_{nw} dx = \frac{1}{|\Omega_i|} \int_{\Omega_i} G(g_w, g_{nw}) dx. \quad (78)$$

We can list the values in all cells, $i = 1, \dots, N$, as vectors $\mathbf{g}_w = [g_{w_1}, \dots, g_{w_N}]^T$ and $\mathbf{g}_{nw} = [g_{nw_1}, \dots, g_{nw_N}]^T$, $\mathbf{F} = [F_1, \dots, F_N]^T$ and $\mathbf{G} = [G_1, \dots, G_N]^T$.

Hence we get

$$\frac{dg_{w_i}}{dt} = F_i(\mathbf{g}_w, \mathbf{g}_{nw}) \quad (79)$$

$$\frac{dg_{nw_i}}{dt} = G_i(\mathbf{g}_w, \mathbf{g}_{nw}) \quad (80)$$

which we can put on a more general form,

$$\mathbf{g}_\alpha = [\mathbf{g}_w, \mathbf{g}_{nw}]^T, \quad (81)$$

$$\mathbf{F}_\alpha = [\mathbf{F}, \mathbf{G}]^T, \quad (82)$$

and hence analyze the set of discrete differential equations

$$\frac{d\mathbf{g}_\alpha}{dt} = \mathbf{F}_\alpha(\mathbf{g}_\alpha). \quad (83)$$

We split the time range into equal partitions of length Δt , i.e.

$$t_{n+1} = t_n + \Delta t, \quad n = 0, \dots, (N - 1) \quad (84)$$

and define \mathbf{v}_α^n as \mathbf{v}_α evaluated at t_n . It is now possible to choose from a number of step methods to evaluate the set of equations, depending on the weighting of \mathbf{F}_α below,

$$\frac{\mathbf{g}_\alpha^{n+1} - \mathbf{g}_\alpha^n}{\Delta t} = \theta \mathbf{F}_\alpha(\mathbf{g}_\alpha^{n+1}) + (1 - \theta) \mathbf{F}_\alpha(\mathbf{g}_\alpha^n). \quad (85)$$

For the discretisation of our set of equations, we will use $\theta = 1$, which corresponds to the implicit backward Euler scheme. $\theta = 1$ gives

$$\frac{\mathbf{g}_\alpha^{n+1} - \mathbf{g}_\alpha^n}{\Delta t} = \mathbf{F}_\alpha(\mathbf{g}_\alpha^{n+1}) \quad (86)$$

In our case, and in all cases when $\theta \neq 0$, the equations are nonlinear and a system of these must be solved using an iterative method. We will apply a Newton method when solving the system of equations, this is the topic of section 7.3.2

Initial Value Discretisations

Since we evaluate the PDE in time, we must include a set of conditions that describe the initial state of the system, a solution v_0 at $t = t_0$. For the coupled system as defined above, the initial conditions can be stated as

$$\mathbf{g}_\alpha(t_0) = [\mathbf{g}_{w0}, \mathbf{g}_{nw0}]^T \quad (87)$$

7.3 Numerical Solvers

After applying the techniques above, we must decide how to solve the discretised system of equations. Equations can be either linear or non-linear, depending on the nature of the problem.

In our case we must solve a set of non-linear equations, although it by adding some simplifying constraints to the pressure- and saturation-dependent variables can be reduced to a linear system, and a linear solver must be applied. We therefore include some theory on solving strategies for both cases.

$$\begin{bmatrix} a_{11} & a_{12} & a_{13} \\ a_{21} & a_{22} & a_{23} \\ a_{31} & a_{32} & a_{33} \end{bmatrix} = \begin{bmatrix} l_{11} & 0 & 0 \\ l_{21} & l_{22} & 0 \\ l_{31} & l_{32} & l_{33} \end{bmatrix} \begin{bmatrix} u_{11} & u_{12} & u_{13} \\ 0 & u_{22} & u_{23} \\ 0 & 0 & u_{33} \end{bmatrix}.$$

Figure 10: A simple LU-factorization

7.3.1 Linear Solver

Solving a linear system of equation on the form

$$Ax = b, \quad A \in \mathbb{R}^{n \times n} \quad x, b \in \mathbb{R}^n \quad (88)$$

has been an area of interest in mathematics for a long time, hence various algorithms have been developed to do so. A typical approach for small systems would be to apply a method that either eliminates the variables stepwise or performs a row reduction, as in the Gaussian method. A typical PDE will consist of a large equation system, but the matrix is sparse, i.e. has a lot of zero entries. For solving these systems, we will in brief consider the well known *L(ower)U(pper)-factorization*, which factors the coefficient matrix A into two triangular matrixes. After applying this factorization, one aims to solve the more manageable system $LUx = b$ by first defining $y = Ux$, then solving $Ly = b$ before inserting this in $Ux = y$ to solve for x .

In our model, we will in the linear case use the solving strategy of *linsolve*, a built in linear solver in MATLAB which performs a LU factorization with partial pivoting, i.e. adding a permutation matrix P , when A is square and a QR factorization with column pivoting otherwise. We will only be concerned with square matrices, so the QR factorisation will not be defined here.

7.3.2 Non-Linear Solver

A system of non-linear equations can be expressed in the form

$$\mathbf{F}(\mathbf{x}) = 0, \quad \mathbf{x} \in \mathbb{R}^n, \quad \mathbf{F} \in \mathbf{C}^1(\Omega), \quad (89)$$

where \mathbf{F} is a continuously differentiable vector-valued function of \mathbf{x} . To solve this system, one can apply *Newton's method*. Newtons method is an iterative method that linearises the system around a point, \mathbf{x}_0 ,

$$\mathbf{F}(x) \approx \mathbf{F}(\mathbf{x}_0) + \mathbf{J}_{\mathbf{F}}(\mathbf{x}_0)(\mathbf{x} - \mathbf{x}_0). \quad (90)$$

$\mathbf{J}_{\mathbf{F}}$ is the Jacobian matrix of the system,

$$\mathbf{J}_{\mathbf{F}}(\mathbf{x}_0) = \begin{bmatrix} \frac{\partial F_1(\mathbf{x}_0)}{\partial x_1} & \cdots & \frac{\partial F_1(\mathbf{x}_0)}{\partial x_n} \\ \vdots & \ddots & \vdots \\ \frac{\partial F_n(\mathbf{x}_0)}{\partial x_1} & \cdots & \frac{\partial F_n(\mathbf{x}_0)}{\partial x_n} \end{bmatrix}. \quad (91)$$

The residual, \mathbf{r}_k , is the calculated system *defect* at step k ,

$$\mathbf{r}_k = \mathbf{F}(\mathbf{x}_k), \quad (92)$$

where we ideally would have $\mathbf{r}_k = 0$. Instead we put a condition on its norm, demanding it to satisfy a given tolerance, $\|\mathbf{r}_k\| < \epsilon$. Applying the Newton iteration, starting from initial value \mathbf{x}_0 , the idea is to estimate \mathbf{x}_{k+1} from

$$\mathbf{x}_{k+1} = \mathbf{x}_k - \mathbf{J}_{\mathbf{F}}^{-1}(\mathbf{x}_k)\mathbf{F}(\mathbf{x}_k). \quad (93)$$

In practice, instead of inverting the Jacobian matrix, we rather solve the system

$$\mathbf{J}_{\mathbf{F}}(\mathbf{x}_k)(\mathbf{x}_{k+1} - \mathbf{x}_k) = -\mathbf{F}(\mathbf{x}_k). \quad (94)$$

Taylor expansion of (90) shows that this method converges quadratically. Newton iterative methods are therefore important tools in solving systems of nonlinear equations. In addition, if the system we are evaluating is by some conditions reduced to a linear system, we can solve equation (88) by defining

$$\mathbf{F}(\mathbf{x}) = \mathbf{A}\mathbf{x} - \mathbf{b} = 0, \quad (95)$$

which makes the Jacobian of \mathbf{F} equal to the matrix \mathbf{A} . Inserting this into the linearised expression,

$$\mathbf{A}(\mathbf{x}_{k+1} - \mathbf{x}_k) = -(\mathbf{A}\mathbf{x}_k - \mathbf{b}) \quad (96)$$

we arrive at

$$\mathbf{A}\mathbf{x}_{k+1} = \mathbf{b}, \quad (97)$$

which tells us; solving a linear system using a Newton method will give us convergence of solutions in one step, regardless of the initial input \mathbf{x}_0 . This can be utilized, although informally, in a checking routine to indicate whether a system is linear or not.

There is however a couple of drawbacks which must be dealt with. Since it converges only locally, one must always be certain that the choice of initial value, \mathbf{x}_0 , is in a neighbourhood of the estimated solution, \mathbf{x} . Also, the Jacobian matrix must be computed for all steps, putting a heavy implementation burden on the programmer. To overcome this, we use automatic differentiation.

7.4 Automatic Differentiation

Automatic differentiation is a tool/technique developed to automatically compute Jacobian matrices. It supplies accurate numerical values of derivatives at points, which in turn can be used in methods that produce numerical

for function	Given:	value-and-derivative object	
		val	der
$f(x) = c$	$c =$	c	0
$f(x) = x$	$x =$	a	1
$u(x)$	$u =$	$u(a)$	$u'(a)$
$v(x)$	$v =$	$v(a)$	$v'(a)$
	Compute:		
$u(x) * v(x)$	$u * v =$	$u(a) * v(a)$	$u'(a) * v(a) + u(a) * v'(a)$
$\sin(u(x))$	$\sin(u) =$	$\sin(u(a))$	$\cos(u(a)) * u'(a)$

Figure 11: Example of AD operator overloading

estimates of sets of equations. Instead of computing the partial differential matrix \mathbf{J} for each iteration, the respective derivatives are computed every time we evaluate \mathbf{F} at a point, see figure 11. Basic differential rules can without problems be implemented in a numerical setting, hence one performs an *operator overloading*, adding an operation to the regular point evaluation of a function. The idea of AD is to reorganize the input to indicate what derivative is desired in the method, and expand the program operations to produce the derivative value as well as the function value; then store these as *one* object. By nesting operations, we can also compute derivatives of more complex functions.

In our case, we use AD in the multi-variable Newton's method, and thus replace the error-prone manual implementation of the Jacobian matrix. It only requires evaluation of the function, since the overloaded operations return the floating-point derivatives as well.

7.5 Discretising Equations

We now apply the discretisation techniques described in sections 7.1 and 7.2 to the equations in section 5.8.

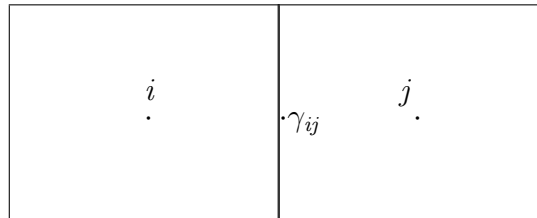


Figure 12: Flux v over face γ_{ij}

Mass Conservation

We discretise the continuity equation

$$\frac{\partial(\phi b_\alpha s_\alpha)}{\partial t} + \nabla \cdot (b_\alpha v_\alpha) = \frac{q_\alpha}{\rho_\alpha S} \quad (98)$$

Spatial Term

We define the *mass* flux as

$$v_{b_\alpha} = b_\alpha v_\alpha, \quad (99)$$

and denote all averaged values on the surface γ_{ij} by the index ij .

For the discretisation of the divergence term, we sum the directional mass flux over all surfaces adjacent to the control volume Ω_i ,

$$\int_{\Omega_i} \nabla \cdot v_{b_\alpha} dx = \sum_j v_{b_\alpha ij} \quad , \forall \Omega_i. \quad (100)$$

Mass flux v_{b_α} over γ_{ij} can be estimated by

$$v_{b_\alpha ij} = - \int_{\gamma_{ij}} b_\alpha \mathbf{K} \frac{k_{r\alpha}}{\mu_\alpha} (\nabla p - g \rho_{\alpha S} b_\alpha \nabla z) \cdot \mathbf{n} ds. \quad (101)$$

We introduce the mobility term as defined in section 3.2.5, $\lambda_\alpha = \frac{k_{r\alpha}}{\mu_\alpha}$. The mobility term consists of the *relative* permeability, which is a function of the phase saturation, and the viscosity, which is a function of pressure and temperature. As mentioned in section 7.1.2, the mobility term makes the equation hyperbolic, and it is the saturation dependency of the relative permeability that is the decisive factor. Using an average value for the mobility will result in inaccurate flux. Instead, we will apply the upstream method to estimate λ_{ij} . We do this by choosing the *saturation*, s_α , upstream

$$s_{\alpha,up} = \begin{cases} s_{\alpha i} & \text{if } v_{\alpha ij} \geq 0 \\ s_{\alpha j} & \text{if } v_{\alpha ij} < 0, \end{cases} \quad (102)$$

hence choosing relative permeability upstream. The mobility term is a function of saturation, therefore also determined upstream

$$\lambda_{\alpha ij} = \frac{k_{r\alpha}(s_{\alpha,up})}{\mu_{\alpha ij}(p, T)}, \quad (103)$$

and denoted as $\lambda_{\alpha,up}$. For the formation volume factor, b_α , that is *outside* the gravitational term, we do the same

$$b_{\alpha ij} = b_{\alpha,up} \quad (104)$$

$$b_{\alpha,up} = \begin{cases} b_{\alpha i} & \text{if } v_{\alpha ij} \geq 0 \\ b_{\alpha j} & \text{if } v_{\alpha ij} < 0 \end{cases} \quad (105)$$

For the b_{α} *inside* the gravitational term, we make a simple face average evaluation. To avoid confusion, the index g is added, indexing the b_{α} inside the gravitational as $b_{\alpha,g}$. The face average is then approximated by

$$b_{\alpha,g,ij} = \frac{(b_{\alpha,g,j} + b_{\alpha,g,i})}{2} \quad (106)$$

We move the upstream evaluated functions out of the integral,

$$v_{b\alpha ij} \simeq -b_{\alpha,up} \lambda_{\alpha,up} \int_{\gamma_{ij}} \mathbf{K}(\nabla p - g\rho_{\alpha S} b_{\alpha} \nabla z) ds. \quad (107)$$

For the permeability, \mathbf{K}_{ij} , we use the harmonic averaged value

$$\mathbf{K}_{ij} = (\Delta x_i + \Delta x_j) \left(\frac{\Delta x_i}{\mathbf{K}_{i,ij}} + \frac{\Delta x_j}{\mathbf{K}_{j,ij}} \right)^{-1}. \quad (108)$$

Inserting these approximations into the integral, g and $\rho_{\alpha ij S}$ are constants and splitting the integral in two parts gives

$$v_{b\alpha ij} \simeq -b_{\alpha,up} \lambda_{\alpha,up} (\Delta x_i + \Delta x_j) \left(\frac{\Delta x_i}{\mathbf{K}_{i,ij}} + \frac{\Delta x_j}{\mathbf{K}_{j,ij}} \right)^{-1} \left(\int_{\gamma_{ij}} \nabla p ds - (g\rho_{(\alpha S)} b_{\alpha,g,ij}) \int_{\gamma_{ij}} \nabla z ds \right). \quad (109)$$

Pressure and gravitation gradients on surfaces are estimated using the TPFA method

$$\nabla p_{ij} \simeq \frac{2(p_j - p_i)}{\Delta x_i + \Delta x_j}, \quad (110)$$

$$\nabla z_{ij} \simeq \frac{2(z_j - z_i)}{\Delta x_i + \Delta x_j}. \quad (111)$$

In addition, to make the formulation compact, the variables that are evaluated upstream is redefined as the upstream evaluated function, y_{up}

$$y_{up} = b_{\alpha,up} \lambda_{\alpha,up}. \quad (112)$$

Inserting these approximations and integrating over the surface gives us

$$v_{b\alpha ij} \simeq -y_{up} 2|\gamma_{ij}| \left(\frac{\Delta x_i}{\mathbf{K}_{i,ij}} + \frac{\Delta x_j}{\mathbf{K}_{j,ij}} \right)^{-1} \left((p_j - p_i) - g\rho_{(\alpha S)} b_{\alpha,g,ij} (z_j - z_i) \right) \quad (113)$$

where we apply the expression for transmissibilities, t_{ij} from section 7.1.1. This gives us the discrete expression of flux over γ_{ij} as

$$\begin{aligned} v_{b\alpha ij} &\simeq -y_{up}t_{ij} \left((p_j - p_i) - g\rho_{(\alpha S)}b_{\alpha,g,ij}(z_j - z_i) \right) \\ &= y_{up}t_{ij} \left((p_i - p_j) + g\rho_{(\alpha S)}b_{\alpha,g,ij}(z_j - z_i) \right), \end{aligned}$$

hence we have an estimate for the divergence of $v_{b\alpha}$ over cell Ω_i :

$$\sum_j v_{b\alpha ij} \simeq \sum_j y_{up}t_{ij} \left((p_i - p_j) + g\rho_{(\alpha S)}b_{\alpha,g,ij}(z_j - z_i) \right). \quad (114)$$

7.5.1 Source Term

Wells are added through grid cells, either vertically, horizontally or as a combination of both. The cells where the well is *open* are called *perforations*, and we add one well equation for every phase at every perforation. The equations evaluate flow of a phase, q_α , from the well, W to cell, i based on a well index, WI , the phase mobility, λ_α , and the difference in pressure between well and cell,

$$q_{\alpha Wi} = WI_{Wi}\lambda_\alpha(p_W - p_i). \quad (115)$$

The well index is a scalar, calculated using a well model, such as a Peaceman model[2]. This results in a system of n equations with $n+1$ unknowns. To solve this set of equations, we eliminate one of the unknowns, $q_{\alpha Wi}$ or p_W , by assuming either constant *flow rate* or constant *bottom hole pressure* and set the value of before simulation begins. We will be assuming constant bottom hole pressure, bhp, in all our simulations.

The well source term is already on a discretised form and is inserted in the equations as an extra equation per phase in perforation cells, i .

Temporal Term

By definition

$$b_\alpha = b_\alpha(p), \quad s_{nw} = 1 - s_w \quad (116)$$

We therefore consider the temporal term as a function of pressure and saturation

$$g_\alpha(p, s_w) = \phi b_\alpha s_\alpha. \quad (117)$$

ϕ is either constant or a function of pressure, g_α is a function hence

$$\frac{\partial g_\alpha(p, s_{nw})}{\partial t} = -\nabla \cdot v_{b\alpha} + \frac{q_{\alpha Wi}}{\rho_{\alpha,S}}. \quad (118)$$

Applying the Backward Euler Scheme from (7.2) to g_α gives the expression

$$\frac{g_\alpha(p^{n+1}, s_w^{n+1}) - g_\alpha(p^n, s_w^n)}{k} = \sum_j v_{b\alpha,ij} + \frac{q_\alpha W_i}{\rho_{\alpha,S}} \quad (119)$$

for a control volume, Ω_i . The right hand side is evaluated at timestep $n + 1$, k is the timestep length, and the source term is equal to zero when i is not a perforation cell.

7.6 Energy equations

We discretise the two-phase energy equation

$$\frac{\partial}{\partial t} \left(\phi \sum_\alpha \rho_\alpha s_\alpha u_\alpha + (1 - \phi) \rho_r e_r \right) + \nabla \cdot \left(\sum_\alpha (\rho_\alpha v_\alpha h_\alpha) - k_T \nabla T \right) = 0. \quad (120)$$

For simplicity, we define the energy related to concentration as E_c to and the energy flux as E_f , hence

$$\frac{\partial}{\partial t} (E_c) + \nabla \cdot (E_f) = 0. \quad (121)$$

We express the enthalpy, h_α , and internal energy, u_α by using specific heat capacities as in section 5.6, hence

$$h_\alpha = c_{p\alpha} T, \quad u_\alpha = c_{V\alpha} T.$$

When discretising the equations, both will be evaluated upstream. The form of the equations are essentially equal, so we follow much of the same procedure as for the mass conservation law in section 7.5

7.6.1 Spatial Term

The spatial term of the energy equation is divided in three terms, two that governs the enthalpy in the fluid phases and one that governs rock temperature conductivity. For the fluid phase terms, we define the *energy flux* function for phase α

$$v_{h\alpha} = h_\alpha b_\alpha v_\alpha.$$

Energy flux over γ_{ij} is approximated as mass flux, but in addition we have the enthalpy term, h_α , which is evaluated upstream, s.t

$$h_{\alpha ij} = \begin{cases} c_{p\alpha} T_i & \text{if } v_{h\alpha i} \geq 0 \\ c_{p\alpha} T_j & \text{if } v_{h\alpha i} < 0. \end{cases} \quad (122)$$

In the same manner as for mass, we define the upstream evaluated function $y_{h,up}$,

$$y_{h,up} = h_{\alpha,up} y_{up}. \quad (123)$$

with y_{up} as defined in (112). Flux over all cell faces then becomes

$$\sum_j v_{h\alpha ij} = \sum_j y_{h,up} t_{ij} \left((p_i - p_j) + g\rho_{(\alpha S)} b_{\alpha,g,ij} (z_j - z_i) \right) \quad (124)$$

i.e. for both phases

$$\sum_{\alpha} \sum_j y_{h,up} t_{ij} \left((p_i - p_j) + g\rho_{(\alpha S)} b_{\alpha,g,ij} (z_j - z_i) \right). \quad (125)$$

For the conductive term, \mathbf{q}_c we express the flux over surface ij by

$$\mathbf{q}_{c,ij} = \int_{\gamma_{ij}} (-k\nabla T) \cdot \mathbf{n} ds. \quad (126)$$

We approximate k_T in the same manner as for permeability, \mathbf{K} ,

$$k_{Tij} = (\Delta x_i + \Delta x_j) \left(\frac{\Delta x_i}{k_{Ti,ij}} + \frac{\Delta x_j}{k_{Tj,ij}} \right)^{-1}, \quad (127)$$

and apply the TPFA for the gradient of T on edge γ_{ij} ,

$$\nabla T_{ij} = \frac{2(T_j - T_i)}{\Delta x_i + \Delta x_j}. \quad (128)$$

Inserting the approximations and integrating over ij gives

$$\mathbf{q}_{c,ij} \simeq t_{Tij} (T_i - T_j) \quad (129)$$

where t_{Tij} are the conductivity transmissibilities. The discretised spatial part of the energy equation for phase α then becomes

$$\begin{aligned} \nabla \cdot E_f \simeq \sum_j \sum_{\alpha} \left(y_{h,up} t_{ij} \left((p_i - p_j) + g\rho_{(\alpha S)} b_{\alpha,g,ij} (z_j - z_i) \right) \right) \\ + \sum_j t_{Tij} (T_i - T_j). \end{aligned} \quad (130)$$

7.6.2 Source Term

The thermal flow in and out of Ω goes through the perforation cells. The flow is estimated by the same equation as for mass flow, but we now consider temperature instead of pressure,

$$Q_{\alpha Wi} = WI_{Wi}\lambda_{\alpha,up}(T_W - T_i). \quad (131)$$

The well index is the same as when applied to the mass flux expression, mobility is evaluated upstream, and the temperature T_w is set as constant. The source term is then added to the equations that govern flow in the perforation cells, i .

7.6.3 Temporal Term

Due to the definitions of all variables in the temporal term of the energy equation, it is a function of p , s_w and T . We write

$$\frac{\partial E_c(p, s_w, T)}{\partial t} = \frac{\partial}{\partial t} \left(\phi \sum_{\alpha} \rho_{\alpha} s_{\alpha} u_{\alpha} + (1 - \phi) \rho_r e_r \right) \quad (132)$$

and apply the backward Euler method on the LHS, and obtain the discretised energy equation,

$$\frac{E_c(p^{n+1}, s_w^{n+1}, T^{n+1}) - E_c(p^n, s_w^n, T)}{k} = \sum_j v_{h\alpha,ij} + \frac{Q_{\alpha Wi}}{\rho_{\alpha,S}} \quad (133)$$

for a control volume, Ω_i . Like for the mass conservation equation, the right hand side is evaluated at timestep $n + 1$, k is the timestep length, and the source term is equal to zero when i is not a perforation cell.

8 Operator splitting

8.1 Background/Motivation

Being able to solve pdes numerically on a computer enables us to model increasingly more complex phenomena. Given this, the PDEs themselves become more complex and more efficient methods for solving them are needed. When adding terms, i.e. operators, to an equation, the numerical methods previously applied could prove unsuited when handling the new equation. Hence a new method must be developed, which in practice may not be

straightforward. *Operator splitting* represents another approach; the strategy is to split the complex problem into less complex sub-problems and solve these with numerical methods that are well suited for each term.

In addition, after having solved the numerical problems, a major concern is keeping the running time at a minimum. If one is able to develop methods that perform the desired control volume computation in less time than the previous (or competitive) and stay within an acceptable margin of error, it could potentially mean saving days of expensive computations when applied to a larger problem.

Theoretical background

Formally, an *operator* \mathbf{A} , is a mapping from one vector space, V , to another(or onto itself), and is defined

$$\mathbf{A} : V \rightarrow V \quad \forall v \in V \quad (134)$$

It is either linear or non-linear, if linear the following holds

$$\mathbf{A}(\alpha v + \beta w) = \alpha \mathbf{A}(v) + \beta \mathbf{A}(w) \quad \forall \alpha, \beta \in \mathbf{R}, v, w \in V \quad (135)$$

As a simple example of an operator splitting, we consider the general operator \mathbf{A} and the differential equation

$$\frac{du}{dt} + \mathbf{A}u = 0. \quad (136)$$

which can be solved analytically and has general solution

$$u(t) = Ce^{-t\mathbf{A}}. \quad (137)$$

$u(t)$ is unique if a set of initial values is provided.

Assume \mathbf{A} can be written as a sum of N operators, $\mathbf{A} = \mathbf{A}_1 + \mathbf{A}_2 + \dots + \mathbf{A}_N$ and that it is possible and easier to solve the new equations

$$\frac{du}{dt} + \mathbf{A}_i u = 0, \quad u(0) = u_0 \quad i = 1, \dots, N \quad (138)$$

with solutions on the form

$$u_i(t) = u_0 e^{-t\mathbf{A}_i} \quad i = 1, \dots, N \quad (139)$$

Now we partition the time scale by setting $t_n = n\Delta t$; operator splitting is hoping that;

$$u(t_{n+1}) \approx e^{-\Delta t \mathbf{A}_N} \dots e^{-\Delta t \mathbf{A}_2} e^{-\Delta t \mathbf{A}_1} u(t_n) \quad (140)$$

If the operators \mathbf{A}_i commute, then

$$e^{-t\mathbf{A}_N} \dots e^{-t\mathbf{A}_2} e^{-t\mathbf{A}_1} = e^{-t\mathbf{A}} \quad (141)$$

and there is no discrepancy between the split and the exact solution. However for most equations, this is not the case. We set $t = n\Delta t$ and investigate what occurs when we coarsen the time step vector. Ultimately, we hope that

$$\lim_{\Delta t \rightarrow 0} (e^{-\Delta t\mathbf{A}_N} \dots e^{-\Delta t\mathbf{A}_2} e^{-\Delta t\mathbf{A}_1})^n u_0 = e^{-t\mathbf{A}} u_0 = u(t) \quad (142)$$

Although operator splitting methods based on analytical solutions may be attractive from a theoretical point of view, they may not be numerically available or computationally too expensive(to evaluate at all points).

8.2 Application

Our model is set up to be solved by a fully implicit solver and a sequentially split solver. In both cases we will use automatic differentiation to solve the set of equations. In the fully implicit case, we solve the equations for pressure, saturation and temperature simultaneously before making a time step,

$$[p^{n+1}, s^{n+1}, T^{n+1}]^T = \mathbf{F}(p^n, s^n, T^n). \quad (143)$$

\mathbf{F} is here the fully implicit solver scheme(the small T on the LHS is the vector *transpose*). In the split version, we separate the multiphase thermal equation from the flow equations. Pressure and saturation is solved from the phase flow equations, then the equations governing thermal flow is solved using these new values. Numerically this translates to solving

$$[p^{n+1}, s^{n+1}]^T = \mathbf{F}_1(p^n, s^n, T^n) \quad (144)$$

where \mathbf{F}_1 is the first AD solver, returning new solutions for pressure and saturation. We then compute T^{n+1} by inserting these into the second AD solver, \mathbf{F}_2 ,

$$T^{n+1} = \mathbf{F}_2(p^{n+1}, s^{n+1}, T^n) \quad (145)$$

before making a time step.

9 Experiments

9.1 Environment Specifications

All simulations are performed on a Ubuntu 12.04 LTS 64-BIT OS, running an Intel i7 2,67GHz processor. All of the programming work is done using *MATLAB* R2013A, a numerical programming environment and language.

9.2 MRST

In addition to MATLABs own tools and functions, we use the *MATLAB Reservoir Simulation Toolbox*, developed at SINTEF Applied Mathematics. MRST is designed for rapid prototyping and visual demonstration of new simulation methods and consists of two main parts: a core offering basic functionality and single and two-phase solvers, and a set of add-on modules offering more advanced models, viewers and solvers.

9.3 Add-On Modules

We will use the MRST add-on module *ad-fi* in all work. Ad-fi is short for *automatic differentiation-fully implicit*, and the module contains fully implicit solvers implemented using automatic differentiation.

MRST environment

Some time was spent initially becoming familiar with the structure, solvers and visualization tools of MRST. Before setting up the main model, initial experiments was done on the core example script "Flow Solver with capillary pressure". In this example, pressure and saturation equations are constructed from the mass conservation equation. Two-phase incompressible flow is then solved applying a sequentially split solver scheme. In brief, some experimenting was done applying constraints on the norms of the pressure and saturation solutions, changing the of order of solvers and creating scripts that would apply and compare results of various input. The next step was to solve the original problem using a fully implicit AD solver, and then compare the results of the split and fully implicit solutions. This work led to the idea that a splitting should be made in a fully implicit AD solver scheme, then comparing the results of these two AD routines.

9.4 Model Description

The original script of the model was the MRST *exampleOWT*, which is a black-oil fully implicit AD solver handling temperature. It was then expanded to handle flow as defined in the discrete fracture network model, the sequentially split scheme was implemented, finally resulting in a script investigating the thermal flow in more or less water saturated fractures.

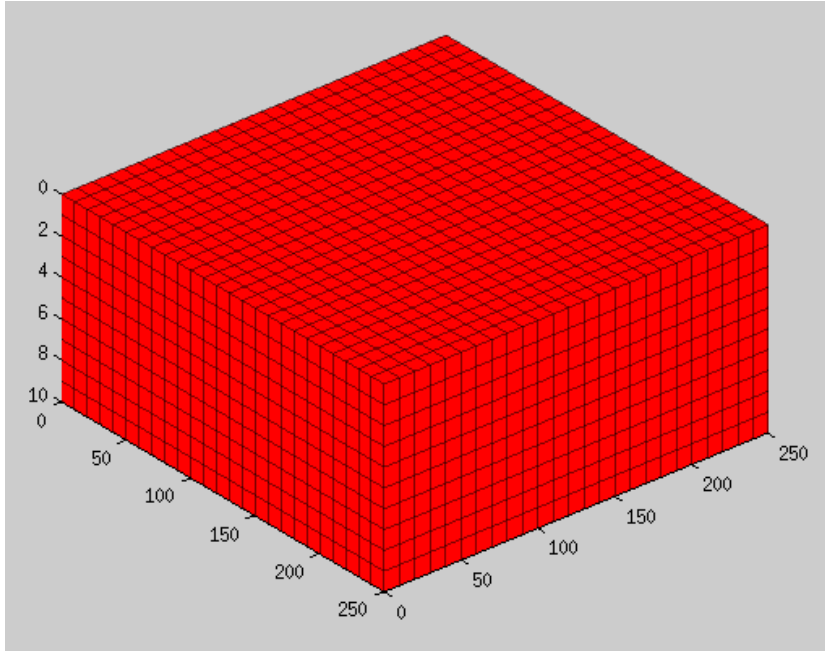


Figure 13: 3D cartesian node grid, visualized by the MRST plotGrid function

9.4.1 Grid

The PDE is solved on a uniform square or cubic Cartesian grid, G , which is divided into control surfaces(2D) or volumes(3D) by equidistant nodes. The geometry of G is stored as a structure, containing information about its cells, nodes and faces.

Fracture implementation

For implementation of fractures as described by DFN model, we add a fracture structure to the cartesian grid, G , by adding a set of connected, evenly distributed vertical surfaces. We first define the fracture density over G . Then, based on the dimensions of G , we identify the cells with surfaces adjacent to the orientation and placing of the fracture surfaces. The information is then stored in vectors, one for each coordinate direction. To calculate the initial fracture permeability, we set an initial fracture "width", b . We then insert b in \mathbf{K} from section 6.2 in order to define the fracture permeability. Although flow in fractures ideally takes place in a open volume, potential sand and sediments must be accounted for. We therefore set the fracture porosity to 0.9. These sediments are loosely connected, and does not transmit heat in between themselves. To include this, or rather not include this effect, we set

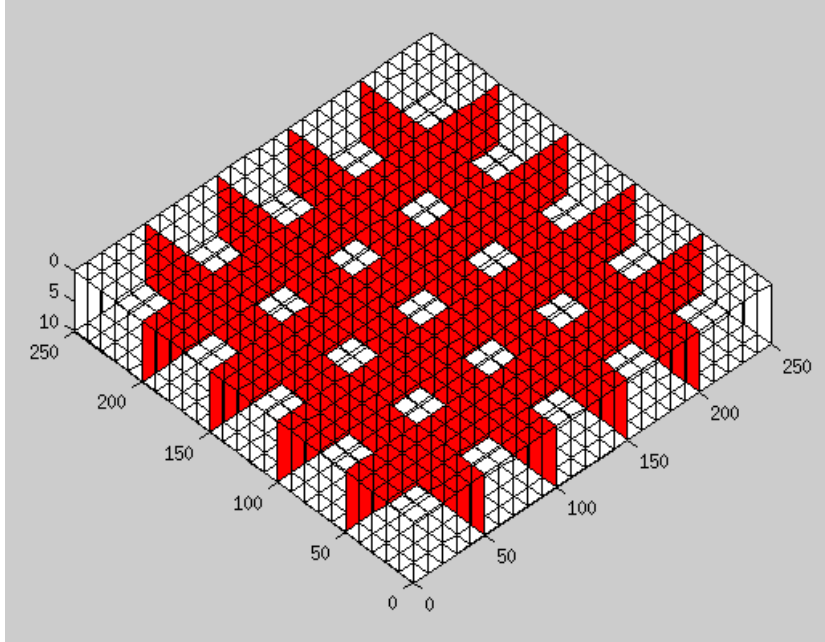


Figure 14: Orthogonal parallel fractures embedded in G

the heat conductivity k_T of the fracture cells to 0. Finally, the vector indices are added to the original grid G as cells, creating a larger grid. The fractures are modelled as an additional structure put "on top of" the original grid, not by adding properties to the original cells in G.

9.4.2 Wells

Since the matrix should be considered almost *impermeable*, we place the vertical wells in cells that are associated with the fractures. The wells are set to have a constant bottom hole pressure, or *bhp*. The injector well, I1, is set to 350 bar and the producer, P1, is set to 100 bar. These values for bhp will be used in all our experiments.

9.4.3 Aperture function

We want to be able to model fracture changes due to changes in reservoir pressure, so we let the fracture aperture, h , be a function of p . We set an initial global reservoir stress, p_s , of 220 bar and define $h(p)$ as

$$h(p) = c_A \frac{(p - p_s)}{p_s} k(p). \quad (146)$$

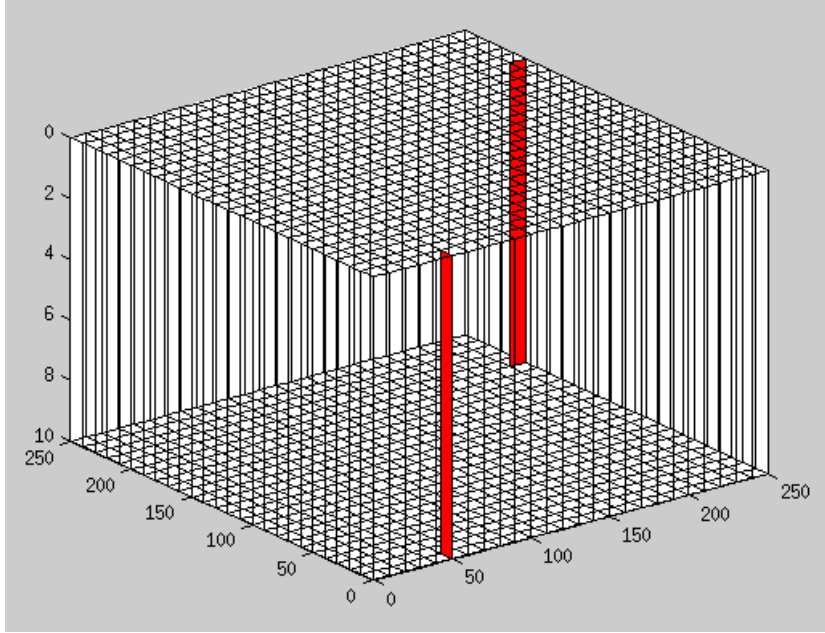


Figure 15: Injector and producer wells set in fractures

$k(p)$ is a characteristic function, defined by

$$k_i = \begin{cases} 1 & \text{if } p > p_s \\ 0 & \text{if } p \leq p_s \end{cases} \quad i = 1, \dots, N, \quad (147)$$

and c_A is an aperture coefficient. We will consider the reservoir stress as homogeneous, meaning that the initial stress p_s is the same in both the fracture and matrix cells. In all our simulations we set $c_A = 10^{-2}$.

9.4.4 Viscosity

The coupling of the mass and energy equations is in the viscosity-function, which is set as a function of pressure and temperature

$$\mu(p, T) = \mu_\alpha(p) e^{-\frac{(T-T_0)}{(T_1-T_0)}}. \quad (148)$$

The *viscosibility*, c_v , indicates the change of phase viscosity with pressure

$$c_{v\alpha} = \frac{1}{\mu_\alpha} \frac{d\mu_\alpha}{dp}, \quad (149)$$

and its SI unit is $1/kPa$. For the incompressible case, $\mu_\alpha(p)$ is a constant function, so $\mu_\alpha(p) = \mu_0$ for all phases. Since water has zero viscosibility,

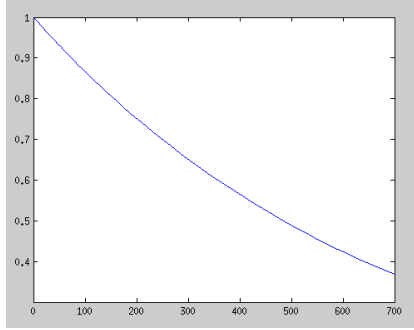


Figure 16: Reynolds function for temperature dependence of $\mu(p, T)$

$\mu_w(p) = \mu_0$ in the compressible single-phase flow case as well. For the study of two-phase compressible flow, we will use oil as secondary phase. $\mu_o(p)$ is expressed by the function

$$\mu_o(p) = e^{c_{vo}(p-p_{ref})} \mu_{o,ref}, \quad (150)$$

where p_{ref} is the set initial reservoir pressure, μ_{or} the reference oil viscosity and c_{vo} the oil viscosibility. All these values are fetched from tables of empirical data, then assembled and assigned to the fluid object. The final expression for oil phase viscosity becomes

$$\mu_o(p, T) = \mu_{o,ref} \frac{e^{c_{vo}(p-p_{ref})}}{e^{\frac{(T-T_0)}{(T_1-T_0)}}}. \quad (151)$$

The coupling is implemented as a an exponential relation which gives a decreasing viscosity for increasing temperatures in the range from 100 to 700 K, as shown in figure 16. This exponential model for the temperature-dependence of shear viscosity was first proposed by Reynolds in 1886.

Although it could be interesting to consider injecting other phases, we will be considering water as injected phase in all our simulations.

9.4.5 Temperature settings

The temperature in the type of reservoirs we are interested in, is in the range of 425-475 K(150-200 degrees Celsius). We therefore set the initial overall reservoir temperature to 450K. The injected phase is set to be 300 K.

9.4.6 Rock properties

We consider granite as our reservoir rock, and apply its standard values for volumetric heat capacity and thermal conductivity, $2170 \text{ kJ}/(m^3K)$ and

2.1 J/mKs respectively. The thermal conductivity, k_T , is calculated and implemented in the same manner as the permeability.

9.4.7 Time keeping routines

To measure the time spent performing the actual calculations in the different cases, we use the MATLAB built-in stopwatch functions *tic* and *toc*. In short, calling the function *tic* starts the stopwatch and calling *toc* stops it. The cue points are set before and after the simulation enters the time step routine, hence the time spent initialising the model is not included in the results listed in the tables below.

9.4.8 Evaluation of temperature solutions

The difference of simulation temperatures between the solvers is evaluated using the infinity norm. The infinity norm represent the largest discrepancy of solutions at each state,

$$\| T_{FI} - T_S \|_{\infty} = \text{ess sup } |T_{FI} - T_S|. \quad (152)$$

9.4.9 Additional Assumptions

In all our cases, we are investigating a system of non-linear equations, and must decide when a solution of it is acceptable. To this end, we must declare a *tolerance* for the residuals, in our case we set it to 10^{-7} .

9.5 Single-Phase Incompressible Flow

We begin with the simplest case, investigating the thermal flow in a 200 x 200 x 10 m reservoir divided into 20 x 20 x 1 control volumes. We consider single-phase, incompressible fluid in a fractured porous medium and investigate the effect of operator splitting. We consider 4 parallel fractures in each horizontal coordinate direction, each fracture is initially completely water saturated. The initial reservoir pressure is set to 234 Bar. The simulation scenarios and results are listed in Table 1.

The initial pressure front moves quickly through the fracture network, creating a pressure drop between injector and producer. Mass flow then follows from the area of high pressure to the area of low pressure. Thermal flow is more slow. The matrix heats the fluid, slowing down the propagation of the cold water front. In figures 17a and 17b we see the thermal flow in both matrix and fractures after 3 and 25 years respectively.

Parameters		Results	
Timespan	Timesteps	Fully Implicit	Op. Split
1 day	20	4.994s	4.406s
100 days	50	10.637s	10.052s
3 years	100	21.032s	20.275s
25 years	250	45.076s	43.934s

Table 1: Single phase incompressible flow scenarios

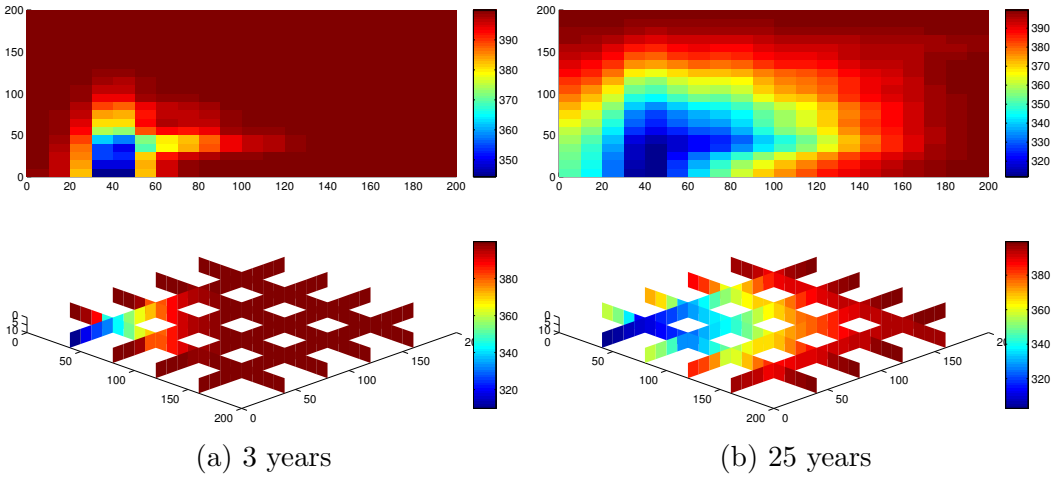


Figure 17: Temperature in matrix and fractures, single phase incompressible flow

We see that the split solver performs the simulation either faster or as fast as the fully implicit solver. However, the fully implicit solver converges in only a few steps, confirming that the routine is efficient and not much computational time can be reduced by introducing a split version for solving the temperature equation.

9.6 Single-Phase Compressible flow

We now expand the properties of our fluid, investigating the compressible case. Density is now a function of pressure, the time scenarios are the same as above.

For the producer cell, if we disregard the fluctuations of temperature solutions during the initial time steps (see figure 24a), the difference of the temperature solutions is relatively small. We see this also on the in the norm plots in Figure 20 and 21

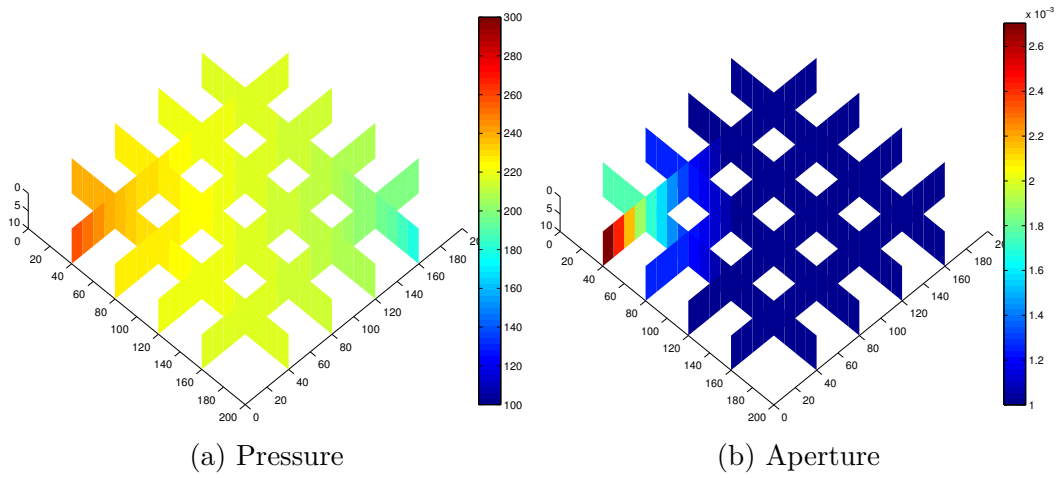


Figure 18: Pressure and aperture in fractures after 25 years of single phase incompressible flow

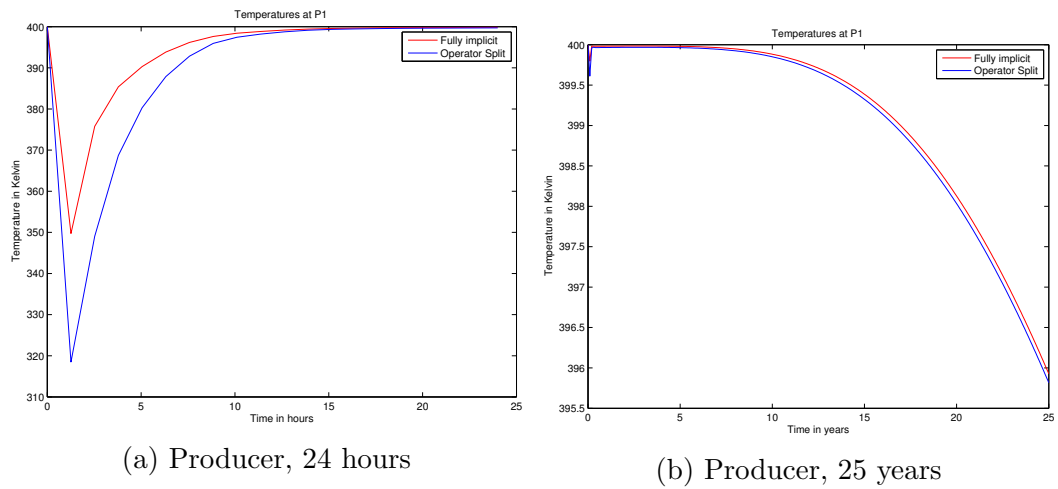


Figure 19: Temperature at Producer cell during 24 hours and 25 years, single phase *incompressible* flow

Parameters		Results	
Timespan	Timesteps	Fully Implicit	Op. Split
1 day	20	5.521	4.953s
100 days	50	10.637s	10.052s
3 years	100	21.032s	20.275s
25 years	250	54.498s	43.184s

Table 2: Single phase *compressible* flow scenarios,

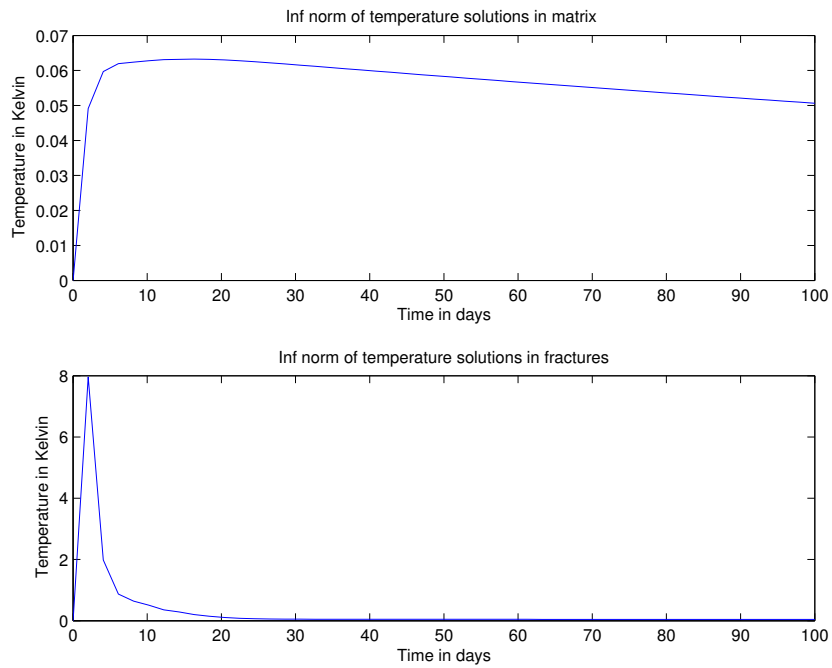


Figure 20: 100 days of simulation incompressible single phase, norm of difference in temperature solutions

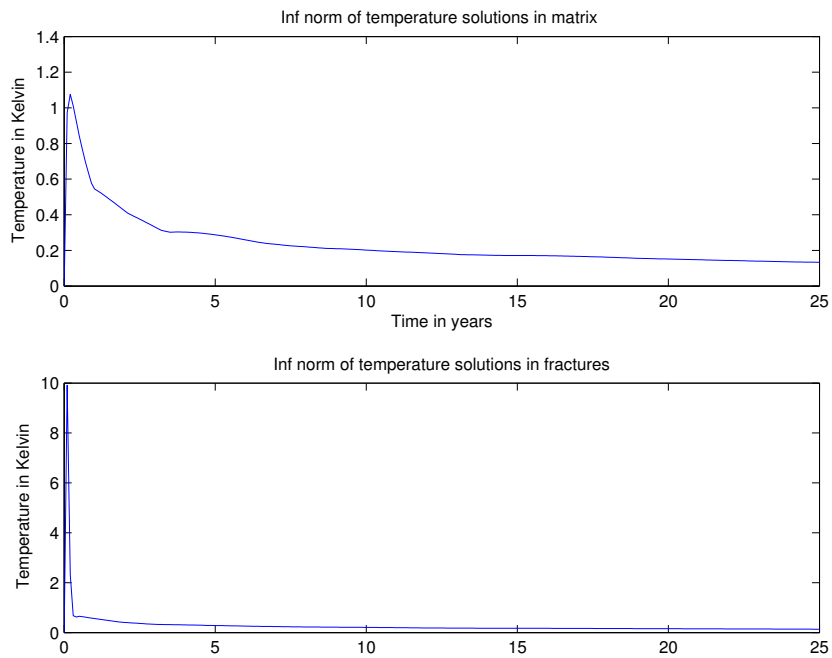


Figure 21: 25 years of simulation incompressible single phase, norm of difference in temperature solutions

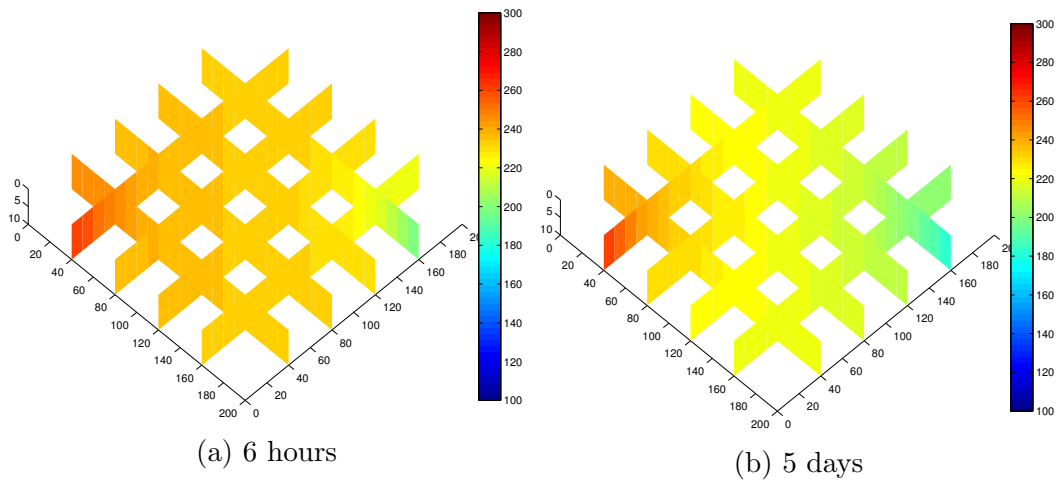


Figure 22: Pressure in fracture after 6 hours and 5 days, single phase *incompressible* flow

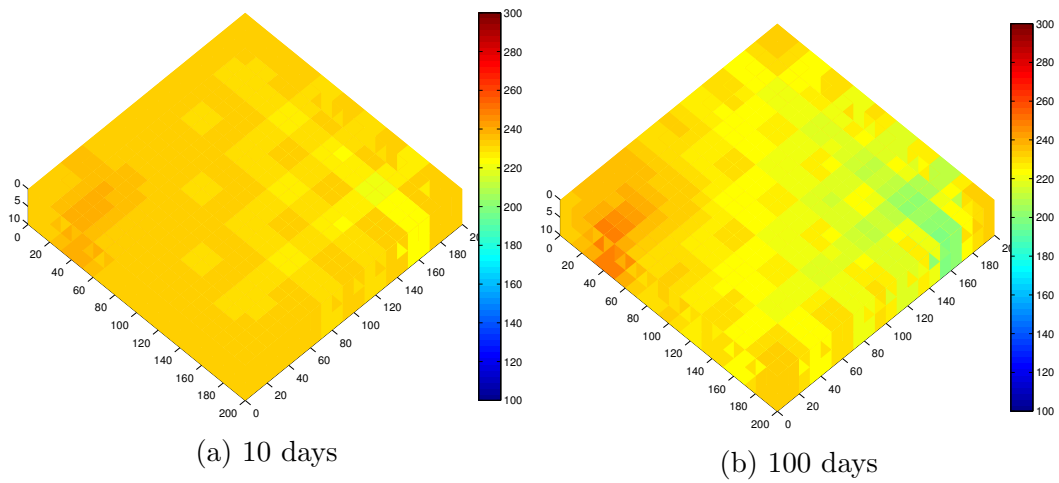


Figure 23: Pressure in matrix after 10 and 100 days, single phase *incompressible* flow

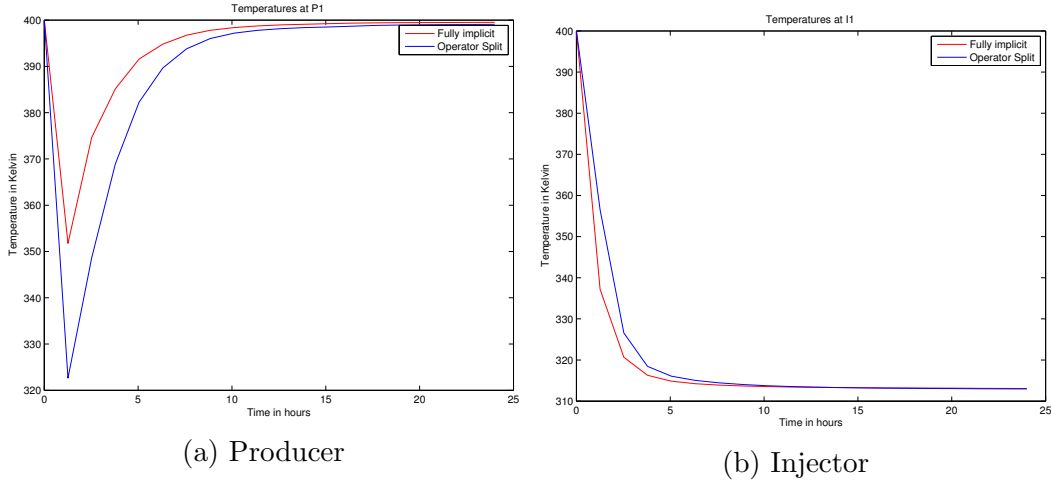


Figure 24: Temperature first 24 hours at Producer and Injector cell, single phase *compressible* flow

We are injecting water in a water saturated fracture network. Water has low compressibility, and we would thus not expect huge differences in the results between the single phase incompressible and compressible cases.

(153)

9.7 Two-Phase Incompressible Flow

In a fractured porous medium, we could have several phases present simultaneously. Water can exist both as a fluid phase and gas phase depending on pressure and temperature, or there could be other fluid and gas phases that effect the thermal flow. Hence, our interest is to simulate how phases interact during different simulation scenarios. Due to the extensive amount of data available, we consider oil as secondary phase. We set the water saturation in fractures to 0.8, and use $\rho_w = 1080\text{kg}/\text{m}^3$ and $\rho_o = 962\text{kg}/\text{m}^3$ as phase densities. In order to ensure convergence, we now introduce differentiated time step vectors. This makes us able to perform more steps per time unit initially, then reduce the frequency as a solution is attained. The viscosity of the oil phase is set to 10 times the viscosity of water.

Saturation

We include a set of saturation plots (figures 32a -32f) showing the water saturation in fractures over a simulation period of 25 years. The oil phase,

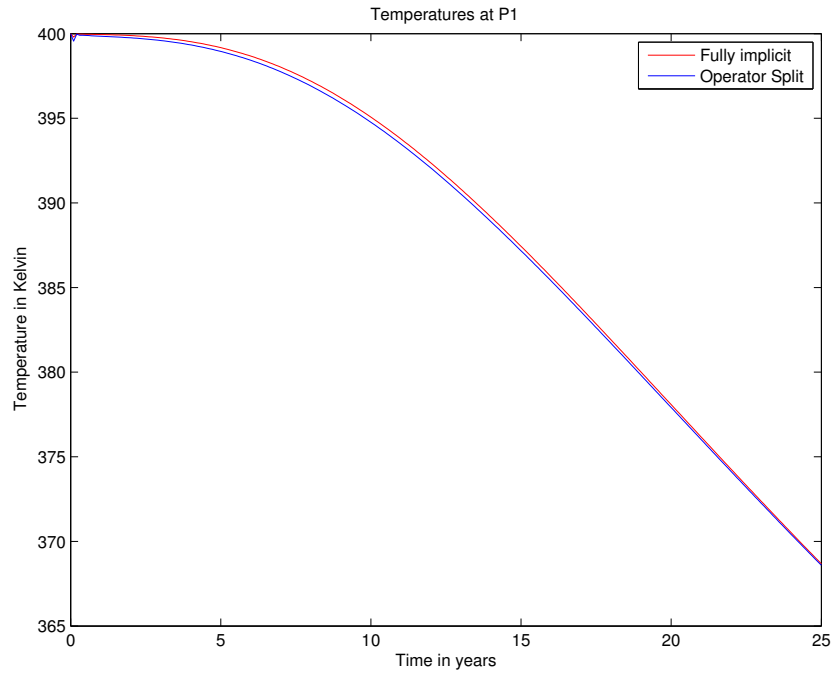


Figure 25: Temperature over 25 years at Producer, single-phase compressible flow

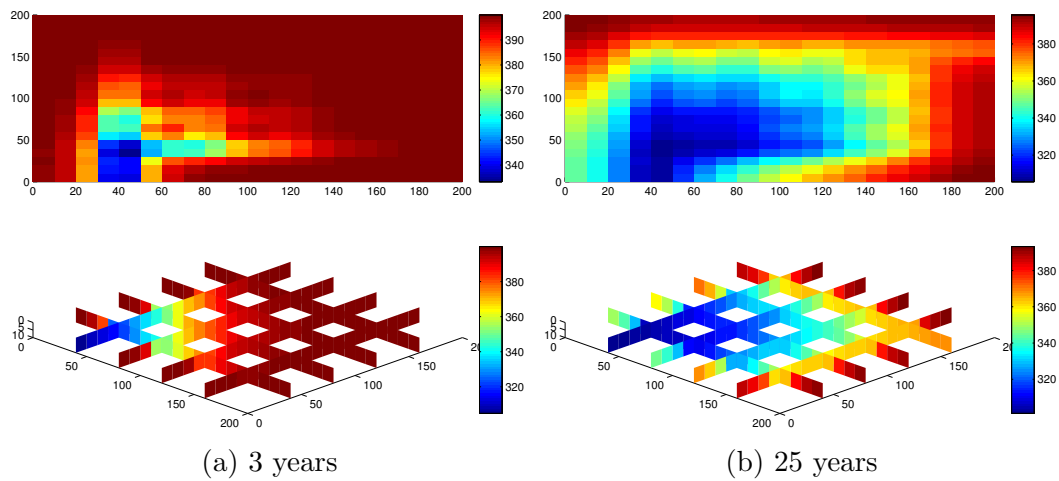


Figure 26: Temperature in matrix and fractures, single phase compressible flow

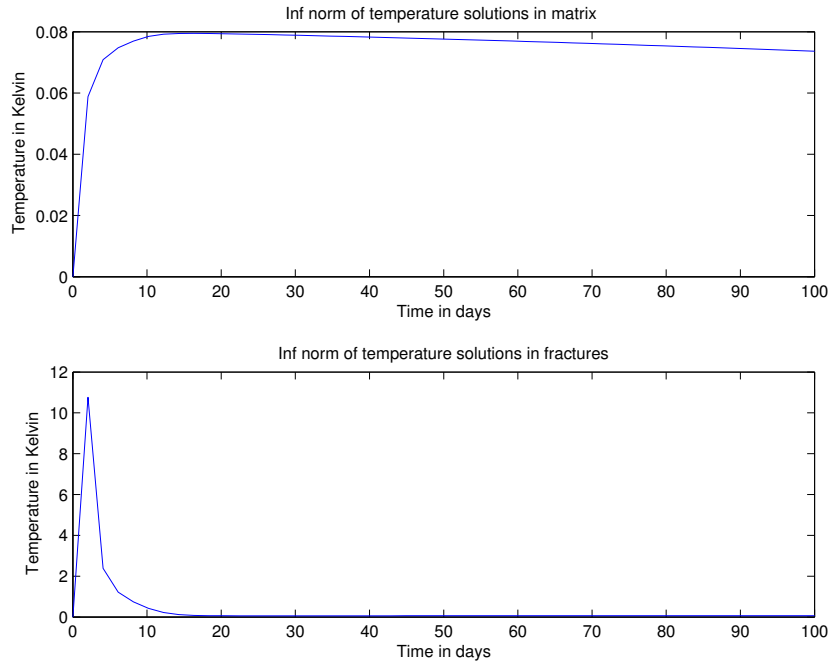


Figure 27: 100 days of simulation incompressible single phase, norm of difference in temperature solutions

being ten times more viscous, is causing a reduction of the mobility of the water phase, hence reducing the total mobility of the system.

Temperature

As we can see from Figure 34, the temperature in producer cell during two-phase simulation is stable for almost the whole simulation period. This shows the effect of relative permeabilities on the total mobility. The water phase mobility is reduced by the much more viscous oil phase present in the fractures. Since we are injecting water phase with constant bottom hole pressure, not constant rate, the thermal conductivity from the hot rocks has a larger effect on the injected phase. The water phase with a lower temperature than the initial reservoir temperature does not reach the producer cell until $t=21$ years. Furthermore, from the plot of the infinity norm of the state temperatures in the fractures, we see that apart from initial peak, the temperature scenarios are relatively equal over the 25 year period. If we compare the fracture norm temperature plots of figure 30 and 34, we see that the initial norm peak is similar. Temperatures of the fully implicit and split solution in the matrix cells are compared above the fracture norm plots. We can see

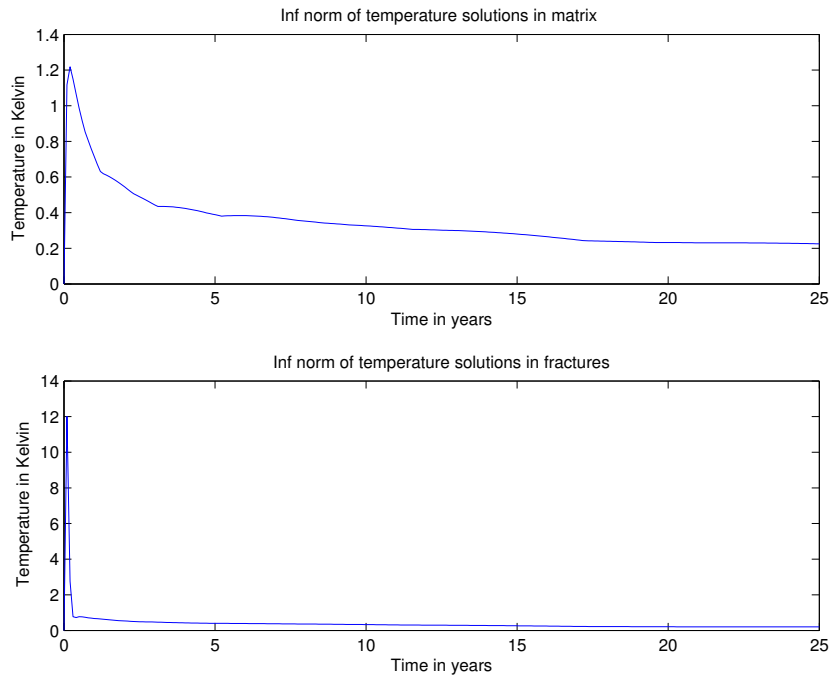


Figure 28: 25 years of simulation incompressible single phase, norm of difference in temperature solutions

that during the 25 year simulation, the difference between solutions is $< 1\text{K}$.

Given the reduced total mobility, the mass flow rate out of the reservoir is reduced. This is again reducing the amount of thermal energy retrieved per time unit at production well, making the production less efficient but more stable.

Grid refinement

For a more precise result, we now increase the number of control volumes in the original grid. This results in more equations to be solved, hence we can expect an increased number of solver iterations before convergence. So far, the fully implicit solver has converged mainly in only two iterations, hence we have not been able to benefit from the convergence speed of split version. We set the physical dimensions as before, but refine the matrix to contain 50 cells in each coordinate direction. We set the number of fractures to 9 in each coordinate direction. The run time results are listed in table 4, and temperature plots included below. The results show that the operator split now is starting to pay off in regards of computational time.

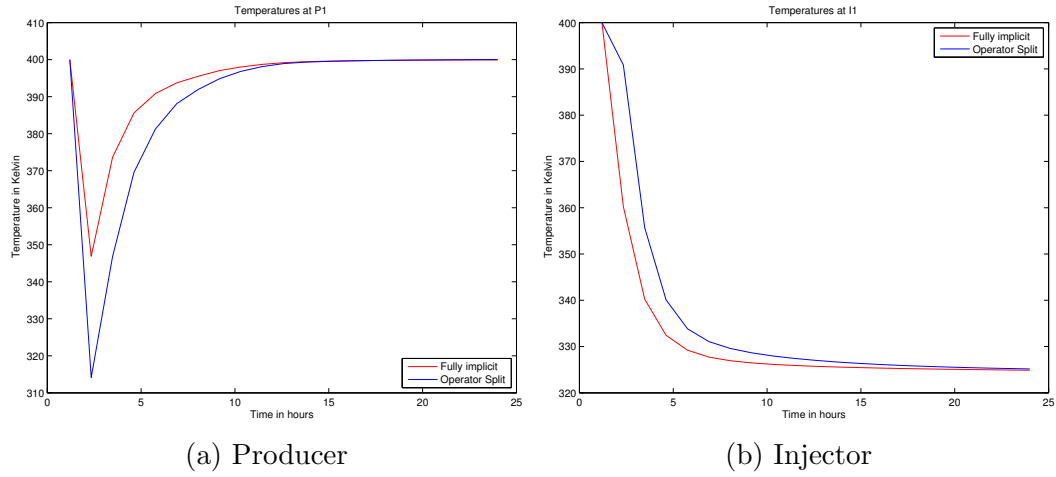


Figure 29: Temperature first 24 hours at Producer and Injector cell, two-phase *incompressible* flow

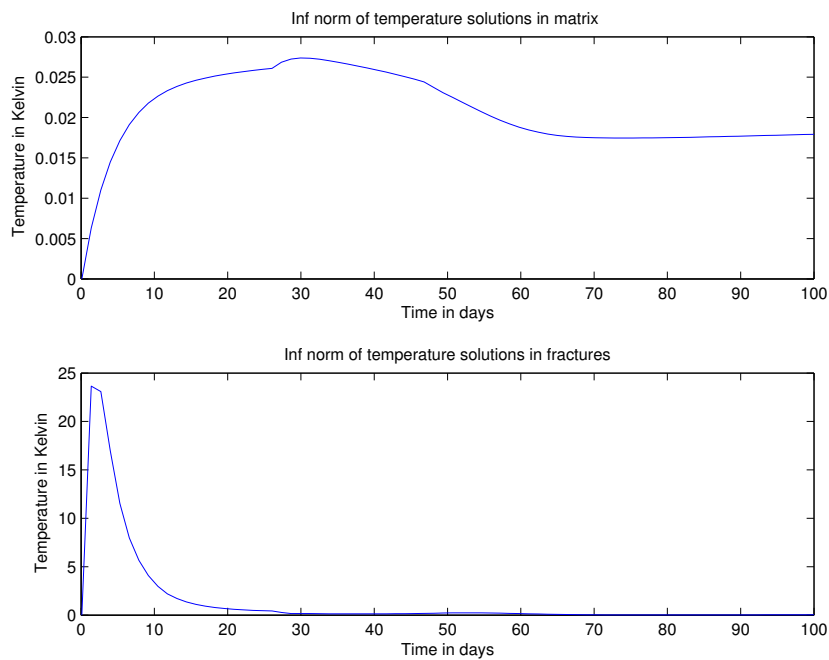


Figure 30: 100 days of simulation incompressible two-phase, norm of difference in temperature solutions

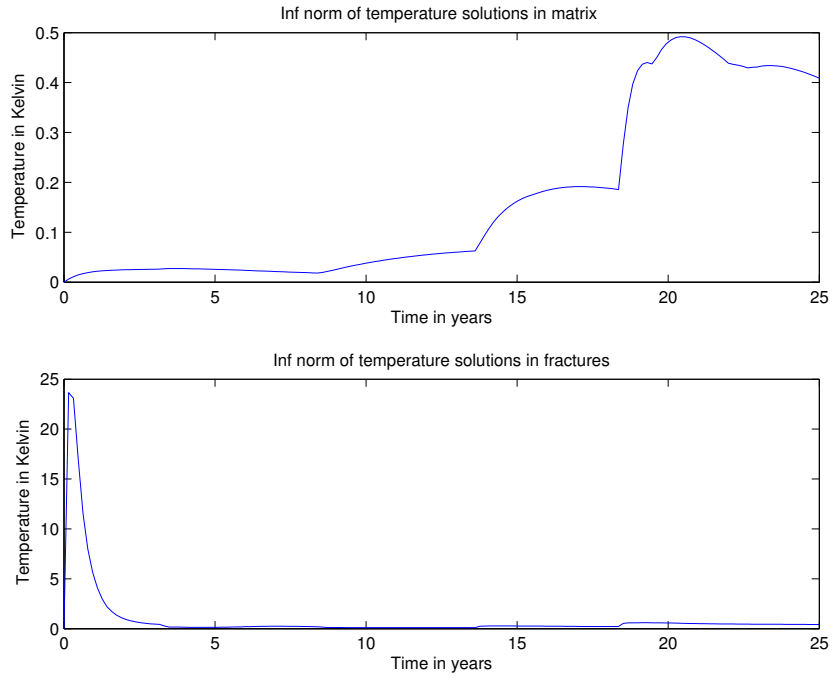


Figure 31: 25 years of simulation, two-phase incompressible flow, norm of difference in temperature solutions

Parameters		Results	
Timespan	Timesteps	Fully Implicit	Op. Split
1 day	20	5.975s	5.181s
100 days	78	16.277s	16.116s
3 years	90	19.496s	19.034s
25 years	158	32.434s	32.084s

Table 3: Two-Phase *incompressible* flow, 4x4 fracture network

Parameters		Results	
Timespan	Timesteps	Fully Implicit	Op. Split
1 day	20	15.323s	13.070s
100 days	78	48.037s	38.019 s
3 years	90	54.625s	43.275s
25 years	158	93.917s	68.629s

Table 4: Two-phase *incompressible* flow, 9x9 fracture network

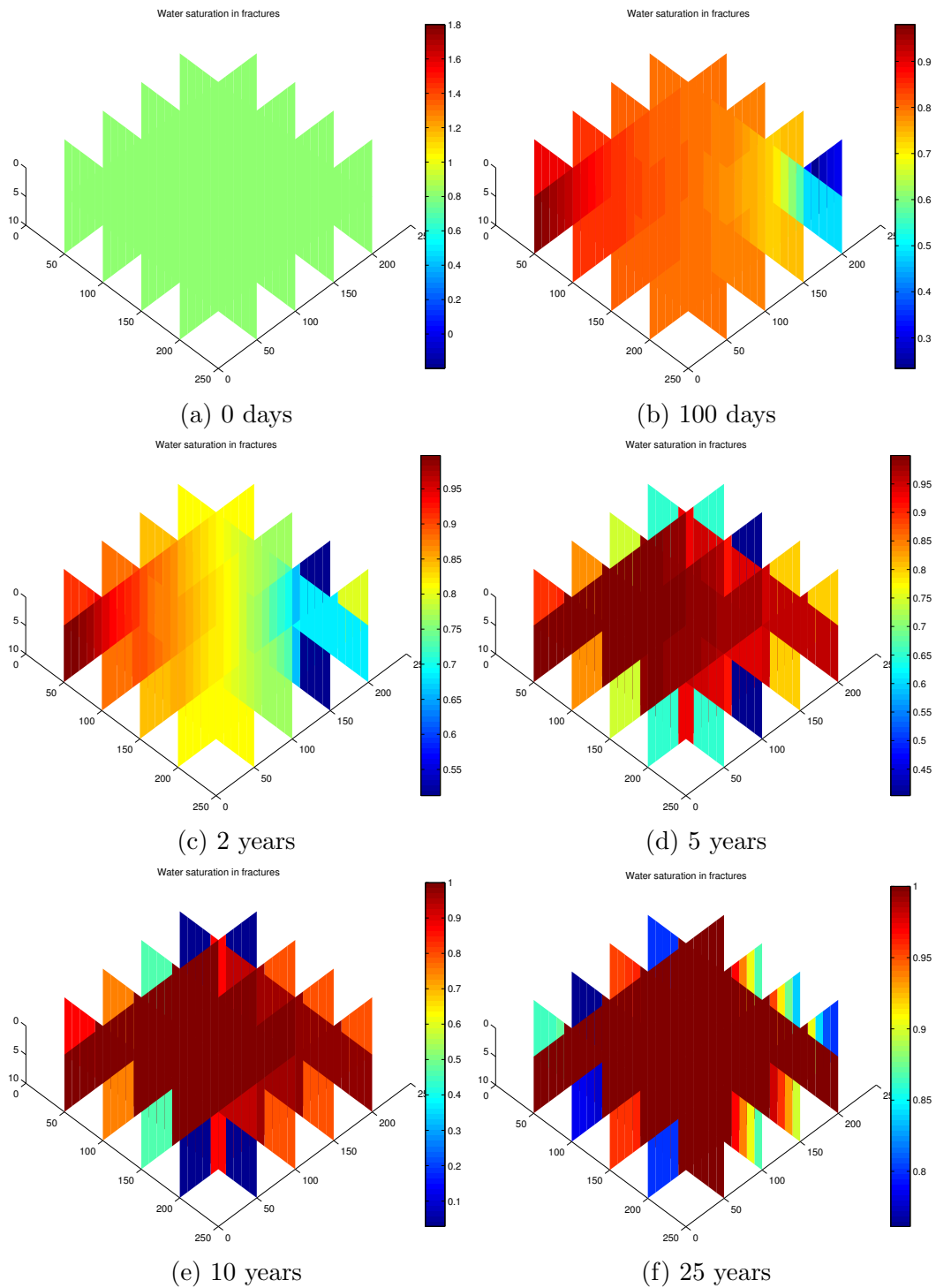


Figure 32: Water saturation in fractures during 25 years of simulation, two-phase *incompressible* flow

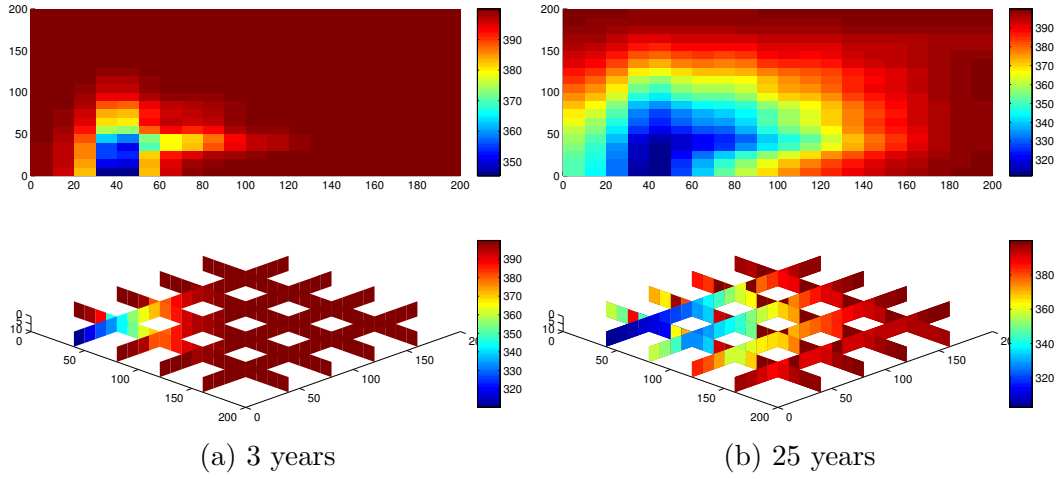


Figure 33: Reservoir and fracture temperatures in two-phase incompressible flow simulation

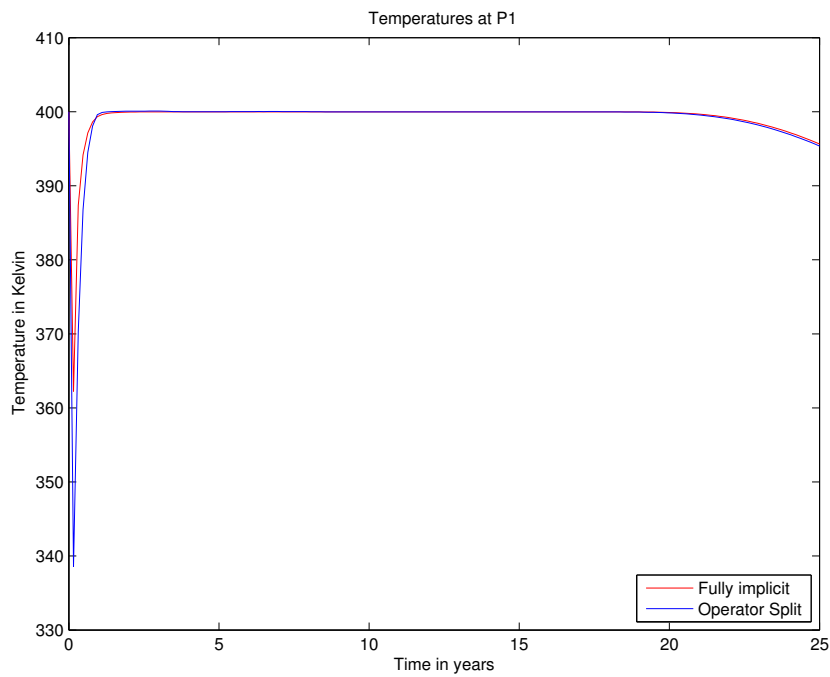


Figure 34: Temperature over 25 years at Producer, two-phase *incompressible* flow

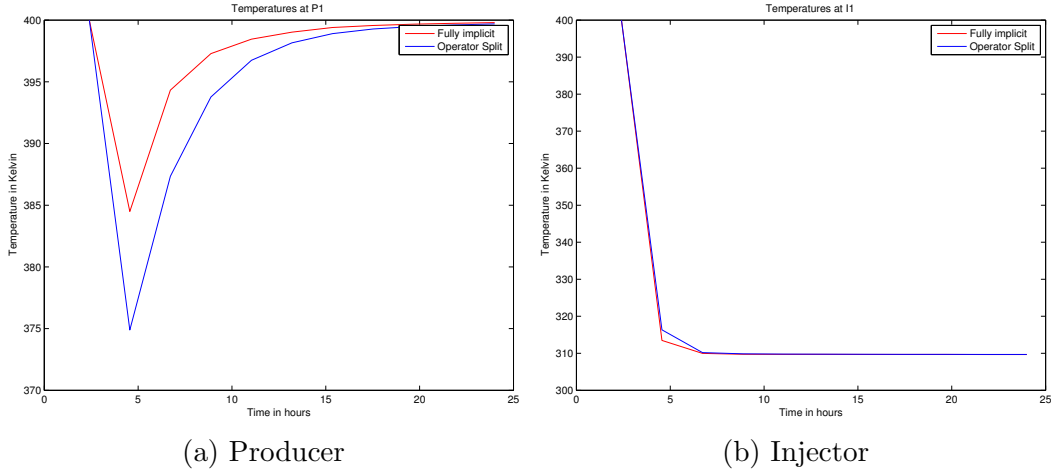


Figure 35: Temperature first 24 hours at Producer and Injector cell, two-phase compressible flow

Parameters		Results	
Timespan	Timesteps	Fully Implicit	Op. Split
1 day	10	14.952s	6.459s
100 days	88	83.534s	55.845s
3 years	85	84.022s	59.247s
25 years	158	149.268s	102.318s

Table 5: Two-Phase *compressible* flow in a 24x24 fracture network

9.8 Two-Phase Compressible Flow

We also include a simulation of two-phase compressible flow, where we consider the a larger physical reservoir and expand the fracture network further. A 250mx250mx10m reservoir is divided into a 50x50x1 matrix cell grid, and combined with a 24x24 fracture network. The properties of oil and water are as with the compressible single phase case fetched and calculated from data. The water saturation is kept at 0.8.

We also include a set of results from investigating two-phase flow with an initial water saturation set to 0.5. The results are listed in table 6, and we see that the results are as we would expect from the previous cases.

As in the previous flow cases, we see that the difference of solutions between the two solvers is relatively small. Since the fracture network is dense, we see that the thermal flow in matrix and fractures(see figures 39a and 39b) are starting to resemble thermal flow as when modelled in an unfractured porous medium.

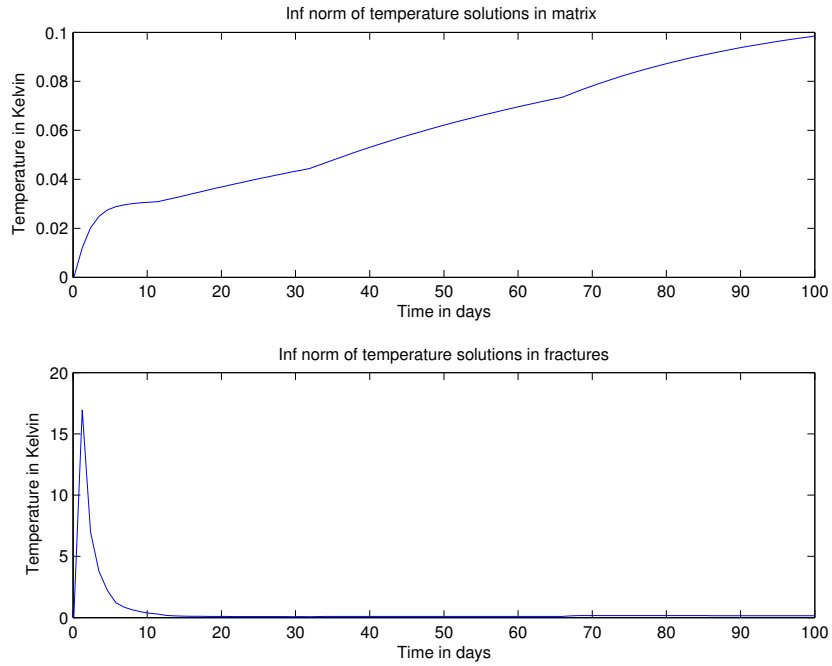


Figure 36: 100 days of simulation compressible two-phase flow, norm of difference in temperature solutions

Parameters		Results	
Timespan	Timesteps	Fully Implicit	Op. Split
1 day	10	16.263 s	8.959 s
100 days	88	90.645	57.390s
3 years	85	89.985s	55.741s
25 years	158	155.558s	102.590s

Table 6: Two-Phase *compressible* flow in a 24x24 fracture network with an initial water saturation set to 0.5

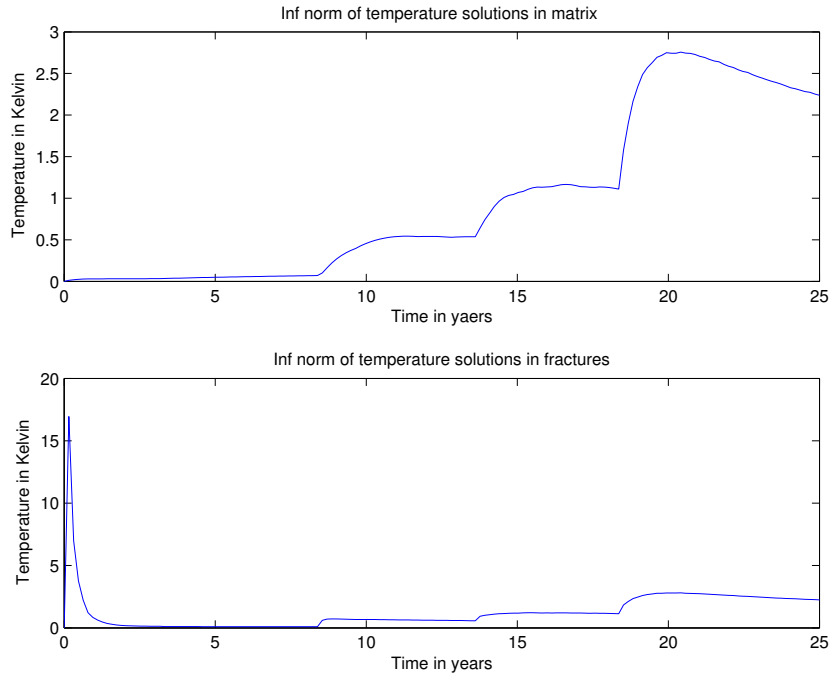
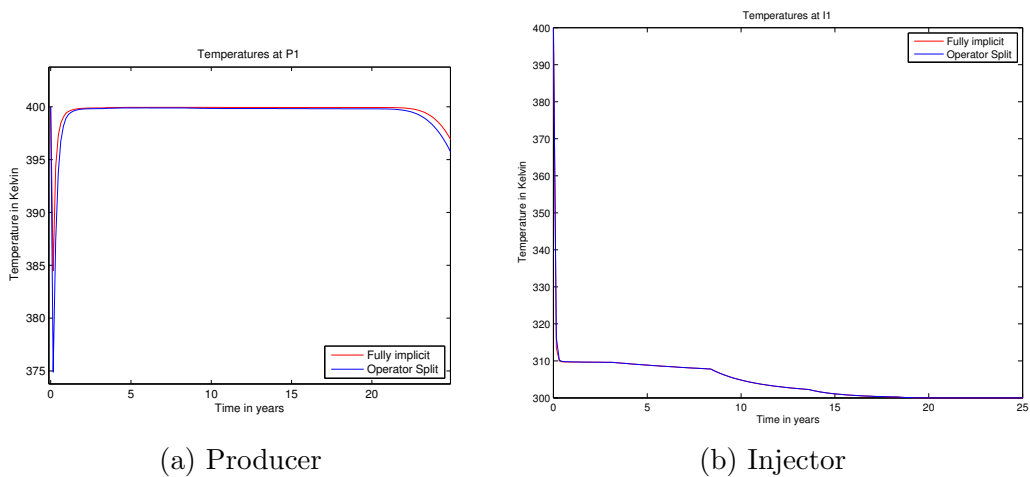


Figure 37: 25 years of simulation compressible two-phase flow, norm of difference in temperature solutions



(a) Producer

(b) Injector

Figure 38: Temperature during 25 years at Producer and Injector cell, two-phase compressible flow

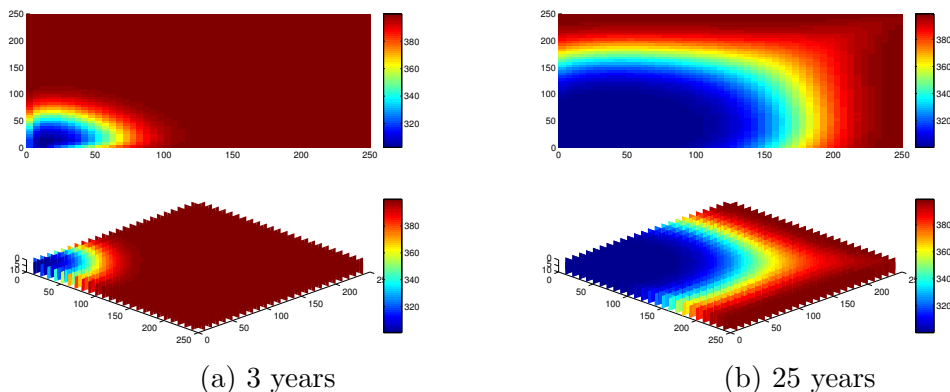


Figure 39: Reservoir and fracture temperatures in two-phase compressible flow simulation

10 Conclusion

From the principle of conservation of mass, momentum and energy, we have derived partial differential equations that govern flow. We have applied numerical methods to these, and the system of discretised partial differential equations has been solved under different conditions using routines implemented in MATLAB.

We begun by simulating incompressible single phase flow in a sparse fracture network and expanded our scenario to finally be simulating two-phase compressible flow in a dense fracture network. During this simulation, our main motivation had been to investigate the differences in temperature solutions produced by the fully implicit and operator split solvers during different flow scenarios.

We have seen that the discrepancies between the two solver schemes are small both in the producer cell and the reservoir as a whole in all fluid flow cases. It should therefore be possible to use the operator split solver scheme for these types of systems. In addition we have seen that the computational benefit from operator splitting is increasing as the simulated system grows more complex.

Future Work

The sequentially split solver returned satisfactory results in terms of running time and error margin compared to the fully implicit solver. It is reasonable to believe that one would benefit further from investigating the application of other and perhaps more efficient splitting techniques. As for the fractures,

the model could be improved by implementing differentiated fracture cell specifications.

An interesting subject of investigation would be the injection of gaseous phases. CO₂ storage is an area of great significance, but it would also be interesting to inject other phases to simulate the thermal flow under different conditions.

Also, in our work we have not looked at the thermal flow as an optimization problem. It would certainly be interesting to investigate the economy aspect of the model, looking at the optimizing of production rates based on short- and long term costs and income.

References

- [1] J.E. Aarnes, T. Gimse, and K.A. Lie. An introduction to the numerics of flow in porous media using matlab. page 40, 2007.
- [2] Z. Chen, G. Huan, and Y. Ma. *Computational Methods for Multiphase Flows in Porous Media*. SIAM, 2006.
- [3] National Research Council. *Rock Fractures and Fluid Flow: Contemporary Understanding and Applications*. National Research Council, 1996.
- [4] D.R. Dowling, I.M. Cohen, and P.K. Kundu. *Fluid Mechanics*. Academic Press, 2012.
- [5] D.E Edwards, C.H adn Penney. *Calculus with analytic geometry*. Prentice Hall, 5th edition, 1998.
- [6] R. Eymard, T. Gallouet, and R. Herbin. *Handbook of Numerical Analysis: Finite Volume Methods*. 2003.
- [7] G. Hasle, K.A. Lie, and E. Quak. *Geometric Modelling, Numerical Simulation and Optimization: Applied Mathematics at SINTEF*. Springer-Verlag, 2007.
- [8] H. Holden, K.H. Karlsen, K.A. Lie, and N.H. Risebro. *Splitting Methods for Partial Differential Equations with Rough Solutions*. European Mathematical Society, 2010.
- [9] Ø. Holter, F. Ingebretsen, and H. Parr. *Fysikk og Energiressurser*. Universitetsforlaget A/S, 2010.
- [10] L.W. Lake. *Enhanced Oil Recovery*. Prentice Hall, 1989.
- [11] V. Lampe. Modelling fluid flow and heat transfer in fractured porous media. Master’s thesis, University of Bergen, 2013.
- [12] J. D. Logan. *Applied Mathematics*. Wiley-Interscience, 2006.
- [13] H.N. More and J.I. DSouaze. Mercury intrusion porosimetry : A tool for pharmaceutical particle characterization. 2013.
- [14] R.D. Neidinger. Introduction to automatic differentiation and matlab object-oriented programming. *SIAM Review*, 52:545–563, 2010.
- [15] Ø. Pettersen. Grunnkurs i reservoarmekanikk. 1990.

- [16] C.E. Robertson. Thermal properties of rocks. *UnitedStates dept of interior, Geological Survey*, 1988.
- [17] T.H. Sandve. *Multiscale simulation of flow and heat transport in fractured geothermal reservoirs*. PhD thesis, UiB, 2012.
- [18] T.H. Sandve, I. Berre, E. Keilegavlen, and J.M. Nordbotten. Multiscale simulation of flow and heat transport in fractured geothermal reservoirs: Inexact solvers and improved transport upscaling. 2013.
- [19] S. Sarkar, N. Toksz, and D.R. Burns. Fluid flow modeling in fractures.
- [20] S. Sarkar, N. Toksz, and D.R. Burns. Fluid flow simulation in fractured reservoirs.
- [21] D.V. Schroeder. *An Introduction to Thermal Physics*. Addison Wesley Longman, 2000.
- [22] J.L. Troutman. *Variational Calculus and Optimal Control: Optimization with Elementary Convexity*. Springer-Verlag, 1983.
- [23] A. Tveito, H.P. Langtangen, B.F. Nielsen, and X Cai. *Elements of Scientific Computing*. Springer-Verlag, 2010.

Appendices

Appendix A We include here the deduction of a flow velocity equation from it to support the mathematical foundation for the Darcy equation.

For horizontal flow in a circular cylinder with radius R , Navier-Stokes' equation along the cylinder axis(x -coordinate) becomes

$$\mu\left(\frac{d^2u}{dr^2} + \frac{1}{r}\frac{du}{dr}\right) = \frac{dp}{dx}$$

with initial conditions $u = 0$ when $r = R$. We solve this equation and get an expression for the fluid velocity, u , at the radial coordinate, r

$$u(r) = -\frac{1}{4\mu}\frac{dp}{dx}(R^2 - r^2).$$

With the initial conditions as above, the mean velocity becomes

$$\tilde{u}(r) = -\frac{R^2}{8\mu}\frac{dp}{dx}.$$

and the rate of flow translates to

$$Q = \tilde{u}\pi R^2 = -\frac{\pi R^4}{8\mu}\frac{dp}{dx}$$

To apply these equations to porous media, we assume that the pores inside the formation behave like the cylinders above. The formation now consists of n such parallel cylinders with radius R_i for $1 \leq i \leq n$, and the space between the cylinders behave like the matrix. We set the total cross section area, A , of the formation, to be the sum of the cross section of the cylinder and matrix area, hence the sum of cylinder surfaces in this slice is less than or equal to A .

This gives us the following expression for the mean flow rate, Q , of the whole model

$$Q = \frac{1}{A}\sum_{i=1}^n Q_i = -\frac{\pi}{8\mu A}\left(\sum_{i=1}^n R_i^4\right)\frac{dp}{dx}.$$

From this we can see that the equation has a defined geometrical part

$$\alpha = -\frac{\pi}{8A}\sum_{i=1}^n R_i^4$$

which clearly governs the permeability of the medium. The rate of flow for the whole model can therefore be written as

$$Q = -\frac{\alpha}{\mu} \frac{dp}{dx},$$

Note that the rate Q depends on both the geometry and the pore volume, and has nothing to do with the actual fluid velocity through each cylinder, which varies from cylinder to cylinder and is not an observable quantity.

Appendix B Setting up the pressure equation for two-phase compressible flow. We now take one step back and differentiate the continuity equation of each phase before summing up.

Applying the product rule of differentiation to the temporal term, we get

$$\frac{\partial(\phi\rho_\alpha s_\alpha)}{\partial t} = \rho_\alpha s_\alpha \frac{\partial\phi}{\partial t} + \phi s_\alpha \frac{\partial\rho_\alpha}{\partial t} + \rho_\alpha \phi \frac{\partial s_\alpha}{\partial t}, \quad (154)$$

whilst the spatial term becomes

$$\nabla \cdot (\rho_\alpha v_\alpha) = \nabla\rho_\alpha \cdot v_\alpha + \rho_\alpha (\nabla \cdot v_\alpha). \quad (155)$$

After dividing with ρ_α , the continuity equation then is on the form

$$s_\alpha \frac{\partial\phi}{\partial t} + \frac{\phi s_\alpha}{\rho_\alpha} \frac{\partial\rho_\alpha}{\partial t} + \phi \frac{\partial s_\alpha}{\partial t} + \frac{\nabla\rho_\alpha \cdot v_\alpha}{\rho_\alpha} + \nabla \cdot v_\alpha = \frac{q_\alpha}{\rho_\alpha}. \quad (156)$$

We now want to set up the expression so that we can solve it w.r.t. pressure and saturation. Hence, we write out the whole equation for all phases. For convenience, we define the sum of source terms on the RHS as

$$q = \frac{q_w}{\rho_w} + \frac{q_{nw}}{\rho_{nw}}.$$

The two-phase continuity equation becomes

$$\begin{aligned} (s_w + s_{nw}) \frac{\partial\phi}{\partial t} + \frac{\phi s_{nw}}{\rho_{nw}} \frac{\partial\rho_{nw}}{\partial t} + \frac{\phi s_w}{\rho_w} \frac{\partial\rho_w}{\partial t} \\ + \phi \frac{\partial s_w}{\partial t} + \phi \frac{\partial s_{nw}}{\partial t} + \frac{\nabla\rho_w \cdot v_w}{\rho_w} + \frac{\nabla\rho_{nw} \cdot v_{nw}}{\rho_{nw}} + \nabla \cdot (v_w + v_{nw}) = q \end{aligned} \quad (157)$$

Utilizing that $s_w + s_{nw} = 1$, and thus $\frac{\partial s_w}{\partial t} = -\frac{\partial s_{nw}}{\partial t}$ gives us an expression for the system by,

$$\frac{\partial\phi}{\partial t} + \phi \frac{s_{nw}}{\rho_{nw}} \frac{\partial\rho_{nw}}{\partial t} + \phi \frac{s_w}{\rho_w} \frac{\partial\rho_w}{\partial t} + \frac{\nabla\rho_w \cdot v_w}{\rho_w} + \frac{\nabla\rho_{nw} \cdot v_{nw}}{\rho_{nw}} + \nabla \cdot (v_w + v_{nw}) = q, \quad (158)$$

with its corresponding Darcy phase flow velocities

$$v_w = -\mathbf{K} \frac{k_{rw}}{\mu_w} (\nabla p_w - \rho_w G) \quad (159)$$

$$v_{nw} = -\mathbf{K} \frac{k_{rnw}}{\mu_{nw}} (\nabla p_{nw} - \rho_{nw} G). \quad (160)$$

$$\begin{aligned}
c_r \phi \frac{\partial p}{\partial t} + \phi s_{nw} \left(c_{nw} \frac{\partial p_{nw}}{\partial t} - \beta_{nw} \frac{\partial T_{nw}}{\partial t} \right) + \phi s_w \left(c_w \frac{\partial p_w}{\partial t} - \beta_w \frac{\partial T_w}{\partial t} \right) \\
+ \frac{\nabla \rho_w \cdot v_w}{\rho_w} + \frac{\nabla \rho_{nw} \cdot v_{nw}}{\rho_{nw}} + \nabla \cdot (v_w + v_{nw}) = q, \quad (161)
\end{aligned}$$

which we sort wrt partial derivatives

$$\begin{aligned}
c_r \phi \frac{\partial p}{\partial t} + \phi \left(s_{nw} c_{nw} \frac{\partial p_{nw}}{\partial t} + s_w c_w \frac{\partial p_w}{\partial t} \right) - \phi \left(s_{nw} \beta_{nw} \frac{\partial T_{nw}}{\partial t} + s_w \beta_w \frac{\partial T_w}{\partial t} \right) \\
+ \frac{\nabla \rho_w \cdot v_w}{\rho_w} + \frac{\nabla \rho_{nw} \cdot v_{nw}}{\rho_{nw}} + \nabla \cdot (v_w + v_{nw}) = q, \quad (162)
\end{aligned}$$

The next step is to insert the Darcy phase velocities (159) and (160) in which we introduce the phase mobilities $\lambda_\alpha = \frac{k_{r\alpha}}{\mu_\alpha}$, but first a quick reminder about the chain rule of gradients functions u and v ;

$$\nabla u(v(x)) = \frac{du}{dv} \nabla v(x) \quad (163)$$

so for our $\rho_\alpha(p, T)$

$$\nabla \rho_\alpha = \frac{\partial \rho_\alpha}{\partial p_\alpha} \nabla p_\alpha + \frac{\partial \rho_\alpha}{\partial T_\alpha} \nabla T_\alpha = \rho_\alpha (c_\alpha \nabla p_\alpha - \beta_\alpha \nabla T_\alpha), \quad (164)$$

hence, the two terms of 162 involving $\nabla \rho_\alpha$ becomes

$$\frac{\nabla \rho_\alpha \cdot v_\alpha}{\rho_\alpha} = (c_\alpha \nabla p_\alpha - \beta_\alpha \nabla T_\alpha) \cdot v_\alpha$$

Inserting this relation into the equation and rewriting

$$\begin{aligned}
c_r \phi \frac{\partial p}{\partial t} + \phi s_{nw} c_{nw} \frac{\partial p_{nw}}{\partial t} + \phi s_w c_w \frac{\partial p_w}{\partial t} - \phi s_{nw} \beta_{nw} \frac{\partial T_{nw}}{\partial t} - \phi s_w \beta_w \frac{\partial T_w}{\partial t} \\
+ c_{nw} \nabla p_{nw} \cdot v_{nw} - \beta_{nw} \nabla T_{nw} \cdot v_{nw} + c_w \nabla p_w \cdot v_w - \beta_w \nabla T_w \cdot v_w \\
+ \nabla \cdot (v_w + v_{nw}) = q \quad (165)
\end{aligned}$$

rearranging with respect to compressibility and thermal expansion coefficients

$$\begin{aligned}
c_{nw} \left(\phi s_{nw} \frac{\partial p_{nw}}{\partial t} + \nabla p_{nw} \cdot v_{nw} \right) + c_w \left(\phi s_w \frac{\partial p_w}{\partial t} + \nabla p_w \cdot v_w \right) \\
- \beta_{nw} \left(\phi s_{nw} \frac{\partial T_{nw}}{\partial t} + \nabla T_{nw} \cdot v_{nw} \right) - \beta_w \left(\phi s_w \frac{\partial T_w}{\partial t} + \nabla T_w \cdot v_w \right) \\
+ \nabla \cdot (v_w + v_{nw}) + c_r \phi \frac{\partial p}{\partial t} = q \quad (166)
\end{aligned}$$

and finally we insert the phase velocities v_{nw}, v_w

$$\begin{aligned}
& c_{nw} \left(\phi s_{nw} \frac{\partial p_{nw}}{\partial t} - \nabla p_{nw} \cdot \mathbf{K} \lambda_{nw} (\nabla p_{nw} - \rho_{nw} G) \right) \\
& \quad + c_w \left(\phi s_w \frac{\partial p_w}{\partial t} - \nabla p_w \cdot \mathbf{K} \lambda_w (\nabla p_w - \rho_w G) \right) \\
& \quad - \beta_{nw} \left(\phi s_{nw} \frac{\partial T_{nw}}{\partial t} - \nabla T_{nw} \cdot \mathbf{K} \lambda_{nw} (\nabla p_{nw} - \rho_{nw} G) \right) \\
& \quad - \beta_w \left(\phi s_w \frac{\partial T_w}{\partial t} - \nabla T_w \cdot \mathbf{K} \lambda_w (\nabla p_w - \rho_w G) \right) \\
& \quad - \nabla \cdot [\mathbf{K} \lambda_w (\nabla p_w - \rho_w G) + \mathbf{K} \lambda_{nw} (\nabla p_{nw} - \rho_{nw} G)] + c_r \phi \frac{\partial p}{\partial t} = q \quad (167)
\end{aligned}$$

This equation is an extended expression for conservation of mass and momentum in non-isothermal compressible two-phase flow. Depending on what we choose to be our primary variable, we can solve for one of the three pressures included in the equation above by using the definition of capillary pressure ($p_c = p_{nw} - p_w$) and initial reservoir conditions to eliminate the others.